

Analysis of laminated composite structures with embedded piezoelectric sheets by variable kinematic shell elements

Original

Analysis of laminated composite structures with embedded piezoelectric sheets by variable kinematic shell elements / Carrera, Erasmo; Valvano, Stefano. - In: JOURNAL OF INTELLIGENT MATERIAL SYSTEMS AND STRUCTURES. - ISSN 1045-389X. - 28:20(2017), pp. 2959-2987. [10.1177/1045389X17704913]

Availability:

This version is available at: 11583/2670516 since: 2017-12-11T10:58:03Z

Publisher:

London:SAGE PUBLICATIONS LTD Lancaster, PA : Technomic Pub. Co., c1999-

Published

DOI:10.1177/1045389X17704913

Terms of use:

This article is made available under terms and conditions as specified in the corresponding bibliographic description in the repository

Publisher copyright

(Article begins on next page)

Analysis of Laminated Composites Structures with Embedded Piezoelectric sheets by Variable-Kinematic Shell Elements

E. Carrera¹, S. Valvano¹

(1) Department of Mechanical and Aerospace Engineering,
Politecnico di Torino, Turin, Italy

Keywords:

Variable-Kinematic, Equivalent-Single-Layer, Layer-Wise, Finite Element Method, Piezoelectric, Carrera Unified Formulation, Shell.

Author and address for Correspondence

Mr. Stefano Valvano
PhD student,
Department of Mechanical and Aerospace Engineering
Politecnico di Torino,
Corso Duca degli Abruzzi, 24,
10129 Torino, ITALY,
tel +39.011.546.6871, fax +39.011.564.6899
e.mail: stefano.valvano@polito.it

Abstract

In this paper, the static analysis of multilayered shell structure embedding piezoelectric layers is performed using some advanced theories, obtained by expanding the unknown variables along the thickness direction using Equivalent-Single-Layer (ESL) models, Layer-Wise (LW) models, and Variable-Kinematic models. The Variable-Kinematic models permit to reduce the computational cost of the analyses grouping some layers of the multilayered structure with ESL models and keeping the LW models in other zones of the multilayer. This model is here extended to the static analysis of electro-mechanical problems. The used refined models are grouped in the Unified Formulation by Carrera (CUF), and they accurately describe the displacement field, the stress distributions, and the electric potential along the thickness of the multilayered shell. The shell element has nine nodes, and the Mixed Interpolation of Tensorial Components (MITC) method is used to contrast the membrane and shear locking phenomenon. The governing equations are derived from the Principle of Virtual Displacement (PVD) and the Finite Element Method (FEM) is employed to solve them. Cross-ply plates and shells with piezoelectric skins and simply-supported edges, subjected to bi-sinusoidal mechanical or electrical load are analyzed. Various aspect ratios and radius to thickness ratios are considered. The results, obtained with different theories within CUF context, are compared with the elasticity solutions given in the literature. From the results, it is possible to conclude that the shell element based on the CUF is very efficient in the study of electro-mechanical problems of composite structures. The Variable-Kinematic models combining the ESL with the LW models, permit to have a reduction of the computational costs, respect with the full LW theories, preserving the accuracy of the results in localized layers.

1 Introduction

The continuous development of new structural materials, such as layered composite materials and/or piezoelectric layers, leads to increasingly complex designs that require careful analysis. The use of piezoelectric components as electro-mechanical transducers in sensor as well as in actuator applications has been continuously increasing. More recently, piezoelectrics have been considered among the most suitable materials for extending the structural capabilities beyond the purely passive load carrying one. Some examples of the most important applications of these “intelligent” structural components are given in [Inman et al., 2001, Chopra, 2000, Gaudenzi, 2009] for vibration and noise suppression, controlled active deformation is treated in [Preumont et al., 2009], and health monitoring in [Foster, 2009, Roger, 2009]. Analytical solution for general smart structural problems is a very tough task, and they exist, only, for very few specialized and idealized cases. Meanwhile, the finite element method has become the most widely used technique to model various physical processes, including piezoelectricity. The introduction of piezoelectric material into a passive structure naturally leads to a multilayered component, and it has been recognized that classical models are not suitable for an accurate design of such structures, see for example the review article of Noor and Burton [Noor and Burton, 1990]. The analysis of layered composite structures is complicated in practice. Anisotropy, nonlinear analysis as well as complicating effects, such as the C_z^0 - Requirements (zig-zag effects in the displacements and interlaminar continuity for the stresses), the couplings between in-plane and out-of-plane strains, are some of the issues to deal. In most of the practical problems, the solution demands applications of approximated computational methods. An overview of several computational techniques for the analysis of laminated structures can be read in the review articles [Reddy and Robbins, 1994, Varadan and Bhaskar, 1997, Carrera, 2001]. The Finite Element Method (FEM) has a predominant role among the computational techniques implemented for the analysis of layered structures. The majority of FEM theories available in the literature are formulated by axiomatic-type theories. The most common used FEM theory is the classical Kirchhoff-Love theory,

and some examples are given in [Koiter, 1970, Ciarlet and Gratie, 2005]. Another classical plate/shell element is based on the First-order Shear Deformation Theory (FSDT), developed by Pryor and Barker [Pryor and Barker, 1971], Noor [Noor, 1972], Hughes [Hughes and Tezduyar, 1981] and many others. A large variety of plate/shell finite element implementations of higher-order theories (HOT) has been proposed in the last twenty years literature. For multilayered structures, in literature, two kinds of models can be adopted: the Equivalent-Single-Layer (ESL) models, or the Layer-Wise (LW) models. For the ESL models, the variables are independent from the number of layers. Differently, the LW models permit to consider different sets of variables per each layer. In many cases the LW models are more accurate than ESL models; meanwhile, LW theories are more expensive than ESL ones concerning computational costs.

The fundamentals of the modeling of piezoelectric materials have been given in many contributions, in particular in the pioneering works of Mindlin [Mindlin, 1952], EerNisse [EerNisse, 1967], Tiersten and Mindlin [Tiersten and Mindlin, 1962], and in the monograph of Tiersten [Tiersten, 1969]. The embedding of piezoelectric layers into plates and shells sharpens the requirements of an accurate modeling of the resulting adaptive structure due to the localized electro-mechanical coupling, see e.g. the review of Saravanos and Heyliger [Saravanos and Heyliger, 1999]. Therefore, within the framework of two-dimensional approaches, layerwise descriptions have been often proposed either for the electric field only (see e.g. the works of Kapuria [Kapuria, 2004] and of Ossadzew-David and Touratier [Ossadzew-David and Touratier, 2004]) or for both the mechanical and electrical unknowns (e.g. Heyliger et al. [Heyliger et al., 1996]). Ballhause et al. [Ballhause et al., 2005] showed that a fourth order assumption for the displacements leads to the correct closed form solution. They conclude that the analysis of local responses requires at least a layer-wise descriptions of the displacements, see also [D'Ottavio et al., 2006]. Benjeddou et al. [Benjeddou et al., 2002] emphasized that a quadratic electric potential through the plate thickness satisfies the electric charge conservation law exactly. Some of the latest contributions to the Finite Elements (FEs) analysis of piezoelectric plates that includes a First-Order Shear Deformation Theory (FSDT) description of displacements and a Layer-Wise (LW) form of the electric potential was developed by Sheik et al. [Sheik et al., 2001]. The numerical, membrane and bending behavior of FEs that are based on FSDTs were analyzed by Auricchio et al. [Auricchio et al., 2001] in the framework of a suitable variational formulation. Some of the latest contributions to the Finite Elements (FEs) analysis of piezoelectric shells that are based on exact geometry solid-shell element with the first-order 7-parameter equivalent single layer theory was developed by Kulikov et al. [Kulikov and Plotnikova, 2011], and a piezoelectric solid-shell element with a mixed variational formulation and a geometrically nonlinear theory was developed by Klinkel et al. [Klinkel and Wagner, 2008]. An efficient four-node FE with layer-wise mechanics was presented in [Yasin and Kapuria, 2014], therefore some important aspects of modeling piezoelectric active thin-walled structures were treated in [Marinković et al., 2009], and a family of 2D refined equivalent single layer models for multilayered and functionally graded smart magneto-electro-elastic plates was presented in [Milazzo, A, 2014].

In the last years, several efforts have been addressed to make the models more efficient. A possible way is to combine multiple models in the analysis of laminate problems; the issue is to maximize the accuracy keeping when it is possible a reduced computational cost. One of the simple types of multiple model methods, for composite laminates analysis, is the concept of selective ply grouping or sublaminates [Wang and Crossman, 1978, Pagano and Soni, 1983, Jones et al., 1984]. The approach consists of creating some local regions, identified by specific ply or plies, within which accurate stresses are desired. The rest of the plies are identified as a global region or the domain part lying outside the local region. In literature, the local region is often modeled by using 3-D finite elements for each material plies, while the global region can be represented by 3-D finite elements grouped in one or more sublaminates. In the global region, the grouped sublaminates can be modeled with an ESL finite element model. The disadvantage of this approach is the use of the 3-D finite elements. Recently this technique of selective

ply grouping or sublaminae has been employed using only 2-D finite elements for both local region and global region. The authors of the present paper used a variable description in the thickness direction of the displacements, [Pagani et al., , Carrera et al., 2017]. The local region can be described with more accuracy by the use of LW models, meanwhile the global region can be described by ESL models. Both ESL and LW models are described by the use of Legendre polynomials. The continuity of the primary variables between local and global region is immediately satisfied using the Legendre polynomials. In the work by Botshekanan Dehkordi et al. [Botshekanan Dehkordi et al., 2013], a variable description in the thickness direction for the static analysis of sandwich plates was performed. That model was derived from the Reissner-Mixed-Variational-Theorem (RMVT) in order to describe a priori the transverse shear and normal stresses. The transverse stresses were approximated through a mixed LW/ESL approach. The same mixed LW/ESL approach with RMVT was then used in [Botshekanan Dehkordi et al., 2016] for nonlinear dynamic analysis of sandwich plates with flexible core and composite faces embedded with shape memory alloy wires.

In this work, the electro-mechanical analysis of multilayered composite structures with piezoelectric layers is performed with an improved shell finite element with a Variable-Kinematic model. It is based on the Carrera's Unified Formulation (CUF), which was developed by Carrera for multi-layered structures [Carrera, 2002, Carrera, 2003]. Many works have been devoted to the extension of CUF to electro-mechanical problems, see [Robaldo et al., 2006, Carrera et al., 2007, Carrera and Robaldo, 2010, Cinefra et al., 2015b]. Among others, the CUF was extended PVD and RMVT variational statements to piezo-laminated plates, see also [Carrera et al., 2010, Carrera and Nali, 2010b]. Mixed FEs for static and dynamics analysis of piezo-electric plates have been provided in [Carrera and Boscolo, 2007], where only transverse stresses were modeled by RMVT. Mixed FEs with direct evaluation of transverse electric displacement have been provided in [Carrera and Nali, 2010a]. Both Equivalent Single Layer (ESL) and Layer Wise (LW) theories contained in the CUF have been implemented in the shell finite element. A Variable-Kinematic model obtained combining the ESL and LW models are developed. The Mixed Interpolation of Tensorial Components (MITC) method [Bathe and Dvorkin, 1986, Bathe and Brezzi, 1987, Bathe et al., 2003, Huang, 1987] is used to contrast the membrane and shear locking. The governing equations for the electro-mechanical linear static analysis of composite structures are derived from the Principle of Virtual Displacement (PVD), to apply the finite element method. Cross-ply plates with simply-supported edges and subjected to bi-sinusoidal mechanical or electrical loads, multilayered cylindrical shells with simply-supported edges and subjected to bi-sinusoidal mechanical or electrical loads are analyzed. The results, obtained with the different models contained in the CUF, are compared with the exact solution given in literature. This paper is organized as follows: geometrical and constitutive relations for shells are presented in Section 2. In Section 3, an overview of higher-order and advanced shell theories developed within the CUF framework is given. Section 4 gives a brief outline of the FEM approach, whereas, in Section 5, the governing equations in weak form for the electro-mechanical linear static analysis of composite structures are derived from the PVD. In Section 6 a short outline of the different modeling approaches is given, and the explanation of the Variable-Kinematic model is drawn. In Section 7, the results obtained using the proposed CUF theories are discussed. Section 8 is devoted to the conclusions.

2 Preliminaries for electro-mechanical problems for shells

Shells are bi-dimensional structures in which one dimension (in general the thickness in the z direction) is negligible concerning the other two dimensions. The reference system of the shell is indicated in Figure 1.

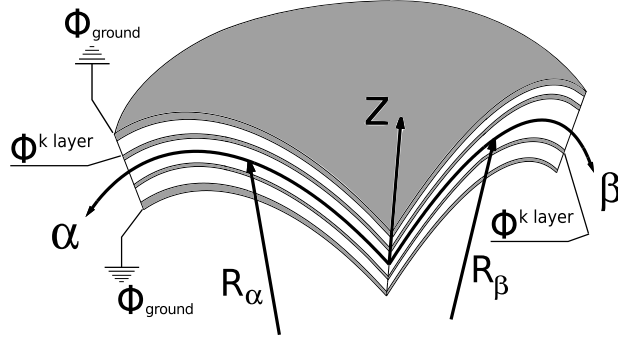


Figure 1: Reference system of the doubly-curved shell.

By considering multilayered structures, the square of an infinitesimal linear segment in the layer, the associated infinitesimal area and volume are given by:

$$\begin{aligned}
 ds_k^2 &= H_\alpha^{k2} d\alpha_k^2 + H_\beta^{k2} d\beta_k^2 + H_z^{k2} dz_k^2, \\
 d\Omega_k &= H_\alpha^k H_\beta^k d\alpha_k d\beta_k, \\
 dV &= H_\alpha^k H_\beta^k H_z^k d\alpha_k d\beta_k dz_k,
 \end{aligned} \tag{1}$$

where the metric coefficients are:

$$H_\alpha^k = A^k(1 + z_k/R_\alpha^k), \quad H_\beta^k = B^k(1 + z_k/R_\beta^k), \quad H_z^k = 1. \tag{2}$$

k denotes the k -layer of the multilayered shell; R_α^k and R_β^k are the principal radii of the mid-surface of the layer k . A^k and B^k are the coefficients of the first fundamental form of Ω_k (Γ_k is the Ω_k boundary). In this paper, the attention has been restricted to shells with constant radii of curvature (cylindrical, spherical, toroidal geometries) for which $A^k = B^k = 1$. Details for shells are reported in [Reddy, 1997]. The geometrical relations enable to express the in-plane ϵ_p^k and out-plane ϵ_n^k strains in terms of the displacement \mathbf{u} for each layer k :

$$\epsilon_p^k = [\epsilon_{\alpha\alpha}^k, \epsilon_{\beta\beta}^k, \epsilon_{\alpha\beta}^k]^T = (\mathbf{D}_p^k + \mathbf{A}_p^k) \mathbf{u}^k, \quad \epsilon_n^k = [\epsilon_{\alpha z}^k, \epsilon_{\beta z}^k, \epsilon_{zz}^k]^T = (\mathbf{D}_{n\Omega}^k + \mathbf{D}_{nz}^k - \mathbf{A}_n^k) \mathbf{u}^k. \tag{3}$$

The explicit form of the introduced arrays is:

$$\mathbf{D}_p^k = \begin{bmatrix} \frac{\partial_\alpha}{H_\alpha^k} & 0 & 0 \\ 0 & \frac{\partial_\beta}{H_\beta^k} & 0 \\ \frac{\partial_\beta}{H_\beta^k} & \frac{\partial_\alpha}{H_\alpha^k} & 0 \end{bmatrix}, \quad \mathbf{D}_{n\Omega}^k = \begin{bmatrix} 0 & 0 & \frac{\partial_\alpha}{H_\alpha^k} \\ 0 & 0 & \frac{\partial_\beta}{H_\beta^k} \\ 0 & 0 & 0 \end{bmatrix}, \quad \mathbf{D}_{nz}^k = \begin{bmatrix} \partial_z & 0 & 0 \\ 0 & \partial_z & 0 \\ 0 & 0 & \partial_z \end{bmatrix}, \tag{4}$$

$$\mathbf{A}_p^k = \begin{bmatrix} 0 & 0 & \frac{1}{H_\alpha^k R_\alpha^k} \\ 0 & 0 & \frac{1}{H_\beta^k R_\beta^k} \\ 0 & 0 & 0 \end{bmatrix}, \quad \mathbf{A}_n^k = \begin{bmatrix} \frac{1}{H_\alpha^k R_\alpha^k} & 0 & 0 \\ 0 & \frac{1}{H_\beta^k R_\beta^k} & 0 \\ 0 & 0 & 0 \end{bmatrix}. \tag{5}$$

The geometrical relations between electric field \mathcal{E} and potential Φ are defined as follows:

$$\begin{aligned}
 \mathcal{E}_p^k &= [\mathcal{E}_\alpha^k, \mathcal{E}_\beta^k]^T = -\mathbf{D}_{ep} \Phi, \\
 \mathcal{E}_n^k &= [\mathcal{E}_z^k]^T = -\mathbf{D}_{en} \Phi,
 \end{aligned} \tag{6}$$

Where the differential operators are defined as follows:

$$\mathbf{D}_{ep} = \begin{bmatrix} \frac{\partial_\alpha}{H_\alpha} \\ \frac{\partial_\beta}{H_\beta} \end{bmatrix}, \quad \mathbf{D}_{en} = [\partial_z].$$

The definition of the constitutive equations that permit to express the stresses σ and the electric displacements \mathcal{D} in terms of the strains and the electric fields is defined as follows:

$$\begin{aligned} \sigma_{pC}^k &= [\sigma_{\alpha\alpha}^k, \sigma_{\beta\beta}^k, \sigma_{\alpha\beta}^k] = \mathbf{C}_{pp}^k \epsilon_{pG}^k + \mathbf{C}_{pn}^k \epsilon_{nG}^k - \mathbf{e}_{pp}^{kT} \boldsymbol{\mathcal{E}}_{pG}^k - \mathbf{e}_{np}^{kT} \boldsymbol{\mathcal{E}}_{nG}^k \\ \sigma_{nC}^k &= [\sigma_{\alpha z}^k, \sigma_{\beta z}^k, \sigma_{zz}^k] = \mathbf{C}_{np}^k \epsilon_{pG}^k + \mathbf{C}_{nn}^k \epsilon_{nG}^k - \mathbf{e}_{pn}^{kT} \boldsymbol{\mathcal{E}}_{pG}^k - \mathbf{e}_{nn}^{kT} \boldsymbol{\mathcal{E}}_{nG}^k \\ \mathcal{D}_{pC}^k &= [\mathcal{D}_\alpha^k, \mathcal{D}_\beta^k] = \mathbf{e}_{pp}^k \epsilon_{pG}^k + \mathbf{e}_{pn}^k \epsilon_{nG}^k + \boldsymbol{\varepsilon}_{pp}^k \boldsymbol{\mathcal{E}}_{pG}^k + \boldsymbol{\varepsilon}_{pn}^k \boldsymbol{\mathcal{E}}_{nG}^k \\ \mathcal{D}_{nC}^k &= [\mathcal{D}_z^k] = \mathbf{e}_{np}^k \epsilon_{pG}^k + \mathbf{e}_{nn}^k \epsilon_{nG}^k + \boldsymbol{\varepsilon}_{np}^k \boldsymbol{\mathcal{E}}_{pG}^k + \boldsymbol{\varepsilon}_{nn}^k \boldsymbol{\mathcal{E}}_{nG}^k \end{aligned} \quad (7)$$

where

$$\mathbf{C}_{pp}^k = \begin{bmatrix} C_{11}^k & C_{12}^k & C_{16}^k \\ C_{12}^k & C_{22}^k & C_{26}^k \\ C_{16}^k & C_{26}^k & C_{66}^k \end{bmatrix}, \quad \mathbf{C}_{pn}^k = \begin{bmatrix} 0 & 0 & C_{13}^k \\ 0 & 0 & C_{23}^k \\ 0 & 0 & C_{36}^k \end{bmatrix} \quad (8)$$

$$\mathbf{C}_{np}^k = \begin{bmatrix} 0 & 0 & 0 \\ 0 & 0 & 0 \\ C_{13}^k & C_{23}^k & C_{36}^k \end{bmatrix}, \quad \mathbf{C}_{nn}^k = \begin{bmatrix} C_{55}^k & C_{45}^k & 0 \\ C_{45}^k & C_{44}^k & 0 \\ 0 & 0 & C_{33}^k \end{bmatrix}$$

$$\mathbf{e}_{pp}^k = \begin{bmatrix} 0 & 0 & 0 \\ 0 & 0 & 0 \end{bmatrix}, \quad \mathbf{e}_{pn}^k = \begin{bmatrix} e_{15}^k & e_{14}^k & 0 \\ e_{25}^k & e_{24}^k & 0 \end{bmatrix}, \quad (9)$$

$$\mathbf{e}_{np}^k = [e_{31}^k \quad e_{32}^k \quad e_{36}^k], \quad \mathbf{e}_{nn}^k = [0 \quad 0 \quad e_{33}^k].$$

$$\boldsymbol{\varepsilon}_{pp}^k = \begin{bmatrix} \varepsilon_{11}^k & \varepsilon_{12}^k \\ \varepsilon_{12}^k & \varepsilon_{22}^k \end{bmatrix}, \quad \boldsymbol{\varepsilon}_{pn}^k = \begin{bmatrix} 0 \\ 0 \end{bmatrix}, \quad (10)$$

$$\boldsymbol{\varepsilon}_{np}^k = [0 \quad 0], \quad \boldsymbol{\varepsilon}_{nn}^k = [\varepsilon_{33}^k].$$

For the sake of brevity, the expressions that relate the material coefficients C_{ij} to the Young's moduli E_1, E_2, E_3 , the shear moduli G_{12}, G_{13}, G_{23} and Poisson ratios $\nu_{12}, \nu_{13}, \nu_{23}, \nu_{21}, \nu_{31}, \nu_{32}$ are not given here, they can be found in [Reddy, 1993]. The piezoelectric material is characterized by the piezoelectric coefficients e_{ij} and the permittivity coefficients ε_{ij} , more details can be found in the book of Rogacheva [Rogacheva, 1994].

3 Unified Formulation for Shells

Classical shell models grant good results when thin thickness, homogeneous structures are considered. On the other hand, the analysis of thick shells, multilayered structures may require more sophisticated theories to achieve sufficiently accurate results. As a general guideline, it is clear that the richer the kinematic field, the more accurate the 2D model becomes. The CUF has the capability to expand each displacement variable at any desired order. Each variable can be treated independently from the others, according to the required accuracy. This procedure becomes extremely useful when multifield problems are investigated such as thermoelastic and piezoelectric applications [Cinefra et al., 2015c,

Cinefra et al., 2016, Cinefra et al., 2015a, Cinefra et al., 2015b]. According to the CUF [Carrera, 2003, Carrera, 1999a, Carrera, 1999b], the displacement field and the electric potential can be written as follows:

$$\left\{ \begin{array}{l} u^k(\alpha, \beta, z) = F_0(z) u_0^k(\alpha, \beta) + F_1(z) u_1^k(\alpha, \beta) + \dots + F_N(z) u_N^k(\alpha, \beta) \\ v^k(\alpha, \beta, z) = F_0(z) v_0^k(\alpha, \beta) + F_1(z) v_1^k(\alpha, \beta) + \dots + F_N(z) v_N^k(\alpha, \beta) \\ w^k(\alpha, \beta, z) = F_0(z) w_0^k(\alpha, \beta) + F_1(z) w_1^k(\alpha, \beta) + \dots + F_N(z) w_N^k(\alpha, \beta) \\ \Phi^k(\alpha, \beta, z) = F_0(z) \Phi_0^k(\alpha, \beta) + F_1(z) \Phi_1^k(\alpha, \beta) + \dots + F_N(z) \Phi_N^k(\alpha, \beta) \end{array} \right. \quad (11)$$

In compact form:

$$\mathbf{u}^k(\alpha, \beta, z) = F_s(z) \mathbf{u}_s^k(\alpha, \beta); \quad \delta \mathbf{u}^k(\alpha, \beta, z) = F_\tau(z) \delta \mathbf{u}_\tau^k(\alpha, \beta) \quad \tau, s = 0, 1, \dots, N \quad (12)$$

$$\Phi^k(\alpha, \beta, z) = F_s(z) \Phi_s^k(\alpha, \beta); \quad \delta \Phi^k(\alpha, \beta, z) = F_\tau(z) \delta \Phi_\tau^k(\alpha, \beta) \quad \tau, s = 0, 1, \dots, N \quad (13)$$

where (α, β, z) is the general reference system (see Figure 1), the displacement vector $\mathbf{u} = \{u, v, w\}$ and the electric potential Φ have their components expressed in this system. δ is the virtual variation associated to the virtual work, and k identifies the layer. F_τ and F_s are the thickness functions depending only on z . τ and s are sum indexes and N is the number of terms of the expansion in the thickness direction assumed for the displacements. For the sake of clarity, the superscript k is omitted in the definition of the Legendre polynomials.

3.1 Legendre-like polynomial expansions

The limitations, due to expressing the unknown variables in function of the midplane position of the shell, can be overcome in several ways. A possible solution can be found employing the Legendre polynomials. They permit to express the unknown variables in function of the top and bottom position of a part of the shell thickness. In the case of Legendre-like polynomial expansion models, the displacements and the electric potential are defined as follows:

$$\mathbf{u} = F_0 \mathbf{u}_0 + F_1 \mathbf{u}_1 + F_r \mathbf{u}_r = F_s \mathbf{u}_s, \quad s = 0, 1, r, \quad r = 2, \dots, N. \quad (14)$$

$$\Phi = F_0 \Phi_0 + F_1 \Phi_1 + F_r \Phi_r = F_s \Phi_s, \quad s = 0, 1, r, \quad r = 2, \dots, N. \quad (15)$$

$$F_0 = \frac{P_0 + P_1}{2}, \quad F_1 = \frac{P_0 - P_1}{2}, \quad F_r = P_r - P_{r-2}. \quad (16)$$

in which $P_j = P_j(\zeta)$ is the Legendre polynomial of j -order defined in the ζ -domain: $-1 \leq \zeta \leq 1$. $P_0 = 1$, $P_1 = \zeta$, $P_2 = (3\zeta^2 - 1)/2$, $P_3 = (5\zeta^3 - 3\zeta)/2$, $P_4 = (35\zeta^4 - 30\zeta^2 + 3)/8$.

For the Layer-Wise (LW) models, the Legendre polynomials and the relative top and bottom position are defined for each layer.

3.2 Refined polynomials with Zig-Zag Function

Due to the intrinsic anisotropy of multilayered structures, the first derivative of the displacement variables in the z -direction is discontinuous. It is possible to reproduce the zig-zag effects in the framework of the ESL description by employing the Murakami theory. According to [Murakami, 1986], a zig-zag term can be introduced into equation(14) as follows:

$$\mathbf{u} = F_0 \mathbf{u}_0 + F_1 \mathbf{u}_1 + F_r \mathbf{u}_r + (-1)^k \zeta_k \mathbf{u}_N^k. \quad (17)$$

It can be introduced also into equation(15) as follows:

$$\Phi = F_0 \Phi_0 + F_1 \Phi_1 + F_r \Phi_r + (-1)^k \zeta_k \Phi_N^k. \quad (18)$$

$$0 = \text{top}, \quad 1 = \text{bottom}, \quad r = 2, \dots, N - 1$$

Such theories are called zig-zag theories. The zig-zag function is defined in each layer k , where the adimensional term ζ_k takes value 1 and -1 at the top and the bottom respectively of each layer.

4 Finite Element approximation

Independently from the choice of the thickness functions, a Finite Element Model (FEM) can be formulated. According to the common FEM approximation, the generalized displacements can be expressed as a linear combination of the shape functions. Considering a 9-node finite element, the generalized displacement and electric potential and their variation are defined as follows:

$$\begin{aligned} \mathbf{u}_s &= N_j \mathbf{u}_{s_j} & \delta \mathbf{u}_\tau &= N_i \delta \mathbf{u}_{\tau_i} & \text{with } i, j &= 1, \dots, 9 \\ \Phi_s &= N_j \Phi_{s_j} & \delta \Phi_\tau &= N_i \delta \Phi_{\tau_i} & \text{with } i, j &= 1, \dots, 9 \end{aligned} \quad (19)$$

where \mathbf{u}_{s_j} , Φ_{s_j} , $\delta \mathbf{u}_{\tau_i}$, $\delta \Phi_{\tau_i}$ are the nodal displacements, the electric potential and their virtual variations, and N_i , N_j are the Lagrangian shape functions defined in each node of the finite element. Substituting the compact form of the FEM approximation (Eq. (19)) in the generalized displacement expansion (Eq. (12)) and electric potential expansion (Eq. (13)), one has:

$$\begin{aligned} \mathbf{u}(\alpha, \beta, z) &= F_s(z) N_j(\alpha, \beta) \mathbf{u}_{s_j} & s &= 0, 1, \dots, N \\ \delta \mathbf{u}(\alpha, \beta, z) &= F_\tau(z) N_i(\alpha, \beta) \delta \mathbf{u}_{\tau_i} & \tau &= 0, 1, \dots, N \\ \Phi(\alpha, \beta, z) &= F_s(z) N_j(\alpha, \beta) \Phi_{s_j} & s &= 0, 1, \dots, N \\ \delta \Phi(\alpha, \beta, z) &= F_\tau(z) N_i(\alpha, \beta) \delta \Phi_{\tau_i} & \tau &= 0, 1, \dots, N \end{aligned} \quad (20)$$

Therefore, to overcome the numerical problems related to the shear locking, it is possible to use many computational procedures, such as reduced integration, selective integration [Hughes et al., 1978], and the mixed interpolation of tensorial components (MITC) [Bathe and Dvorkin, 1986]. In this paper, a MITC technique is used to overcome the shear locking phenomenon, for more details see [Cinefra et al., 2015b].

5 Governing FEM equations for electro-mechanical problems

The PVD for a multilayered shell structure reads:

$$\int_{\Omega_k} \int_{A_k} \left\{ \delta \boldsymbol{\epsilon}_{pG}^k \mathbf{T} \boldsymbol{\sigma}_{pC}^k + \delta \boldsymbol{\epsilon}_{nG}^k \mathbf{T} \boldsymbol{\sigma}_{nC}^k - \delta \boldsymbol{\mathcal{E}}_{pG}^k \mathbf{T} \boldsymbol{\mathcal{D}}_{pC}^k - \delta \boldsymbol{\mathcal{E}}_{nG}^k \mathbf{T} \boldsymbol{\mathcal{D}}_{nC}^k \right\} H_\alpha H_\beta d\Omega_k dz = \delta L_e \quad (21)$$

where Ω_k and A_k are the integration domains in the plane and the thickness direction, respectively. The left-hand side of the equation represents the variation of the internal work, while the right-hand side is the virtual variation of the external work. Substituting the constitutive equations (7), the geometrical relations written via the MITC method and applying the CUF (12,13) and the FEM approximation (19), one obtains the following governing equations:

$$\delta \mathbf{u}_{\tau_i}^k : \mathbf{K}_{uu}^{k\tau s i j} \mathbf{u}_{s_j}^k + \mathbf{K}_{u\Phi}^{k\tau s i j} \Phi_{s_j}^k = \mathbf{P}_{u_{s_j}}^k \quad (22)$$

$$\delta \Phi_{\tau_i}^k : \mathbf{K}_{\Phi u}^{k\tau s i j} \mathbf{u}_{s_j}^k + \mathbf{K}_{\Phi\Phi}^{k\tau s i j} \Phi_{s_j}^k = \mathbf{P}_{\Phi_{s_j}}^k \quad (23)$$

In compact form:

$$\delta \mathbf{q}_{\tau i}^k : \mathbf{K}^{k\tau s i j} \mathbf{q}_{s j}^k = \mathbf{P}_{s j}^k \quad (24)$$

where

$$\mathbf{K}^{k\tau s i j} = \begin{bmatrix} \mathbf{K}_{uu} & \mathbf{K}_{u\Phi} \\ \mathbf{K}_{\Phi u} & \mathbf{K}_{\Phi\Phi} \end{bmatrix}^{k\tau s i j} \quad (25)$$

where $\mathbf{K}^{k\tau s i j}$ is a 4×4 matrix, called fundamental nucleus of the mechanical stiffness matrix, and its explicit expression is given in [Cinefra et al., 2015a]. The mechanical part $\mathbf{K}_{uu}^{k\tau s i j}$ is a 3×3 matrix, the coupling matrices $\mathbf{K}_{u\Phi}^{k\tau s i j}$, $\mathbf{K}_{\Phi u}^{k\tau s i j}$ have dimension 3×1 and 1×3 respectively, and the electrical part $\mathbf{K}_{\Phi\Phi}^{k\tau s i j}$ is a 1×1 matrix. The nucleus is the basic element from which the stiffness matrix of the whole structure is computed. The fundamental nucleus is expanded on the indexes τ and s to obtain the stiffness matrix of each layer k . Then, the matrixes of each layer are assembled at the multi-layer level depending on the approach considered. $\mathbf{P}_{s j}^k$ is a 3×1 matrix, called fundamental nucleus of the external load. $\mathbf{q}_{s j}^k$ and $\delta \mathbf{q}_{\tau i}^k$ are the nodal displacements and electric potential and its variation respectively.

6 Modeling Approaches

Two different types of modeling approaches are usually used in literature:

- The Equivalent Single Layer models, here referred to as ESL
- The Layer Wise models, here referred to as LW

In this paper a third modeling approaches is taken into account. It is a variable kinematic model obtained as a combination of the ESL and LW models. The choice of the modeling approach is independent of the type of the used polynomials.

6.1 ESL models

In an ESL model, a homogenization of the properties of each layer is conducted by summing the contributions of each layer in the stiffness matrix. This process leads to a model that has a set of variables that is assumed for the whole multilayer. In this work the ESL model is employed using both Taylor and Legendre polynomials. The ESL assembly procedure of the stiffness matrix in the framework of CUF is shown in Figure 2.

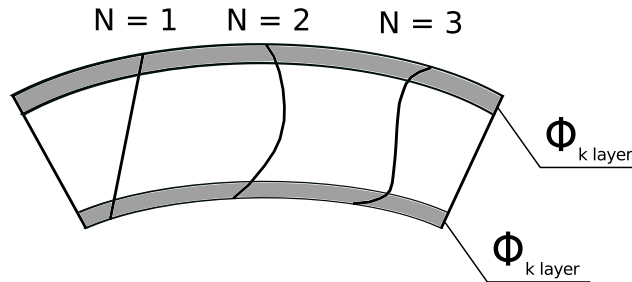


Figure 2: Equivalent-Single-Layer behaviour of the primary variables $\{u, v, w, \Phi\}$ along the thickness of the shell.

6.2 LW models

LW considers different sets of variables per each layer, and the homogenization is just conducted at the interface level. The LW assembly procedure is presented in Figure 3. In this work the LW model

is employed using the Legendre polynomials. The Legendre polynomial F_0 and F_1 interpolate the displacements at the top (t) and bottom (b) position of the layer, respectively. The unknown variables at the top (t) and bottom (b) position are used to impose the following compatibility conditions:

$$\mathbf{u}_t^k = \mathbf{u}_b^{k+1}, \quad k = 1, N_l - 1. \quad (26)$$

$$\Phi_t^k = \Phi_b^{k+1}, \quad k = 1, N_l - 1. \quad (27)$$

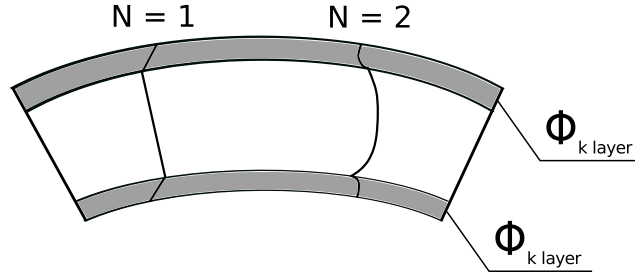


Figure 3: Layer-Wise behaviour of the primary variables $\{u, v, w, \Phi\}$ along the thickness of the shell.

6.3 Variable-Kinematics

In this paper, a different model is taken into account. This Variable-Kinematic model is obtained as a combination of the ESL and LW models. In order to combine these two different models, the Legendre polynomials have been taken into account. In a multilayered structure, some layers can be modeled with a homogenization of the properties and modeled with an ESL assembling procedure, whereas for some layers the homogenization is conducted just at the interface level. This homogenization at the interface level between the ESL and LW models is performed by the use of the Legendre polynomials. The Variable-Kinematic assembling, developed in the framework of the CUF, is very simple to integrate, for example in a FORTRAN code, with few lines of programming. The programming lines of the nucleus equations remain unchanged both for ESL, for LW and Variable Kinematic assembling. The Variable-Kinematic assembly procedure of the stiffness matrix in the framework of CUF is shown in Figure 4. An overview of the assembling scheme of the ESL, LW and Variable-Kinematics approaches is given in Figure 5.

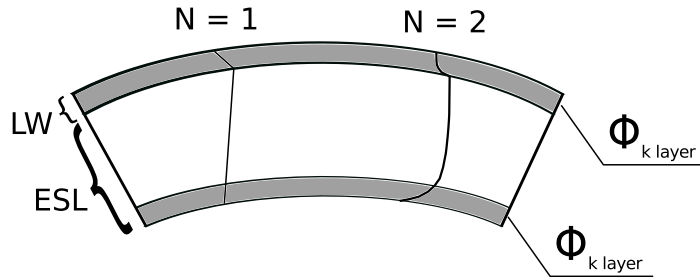


Figure 4: Variable-Kinematics behaviour of the primary variables $\{u, v, w, \Phi\}$ along the thickness of the shell.

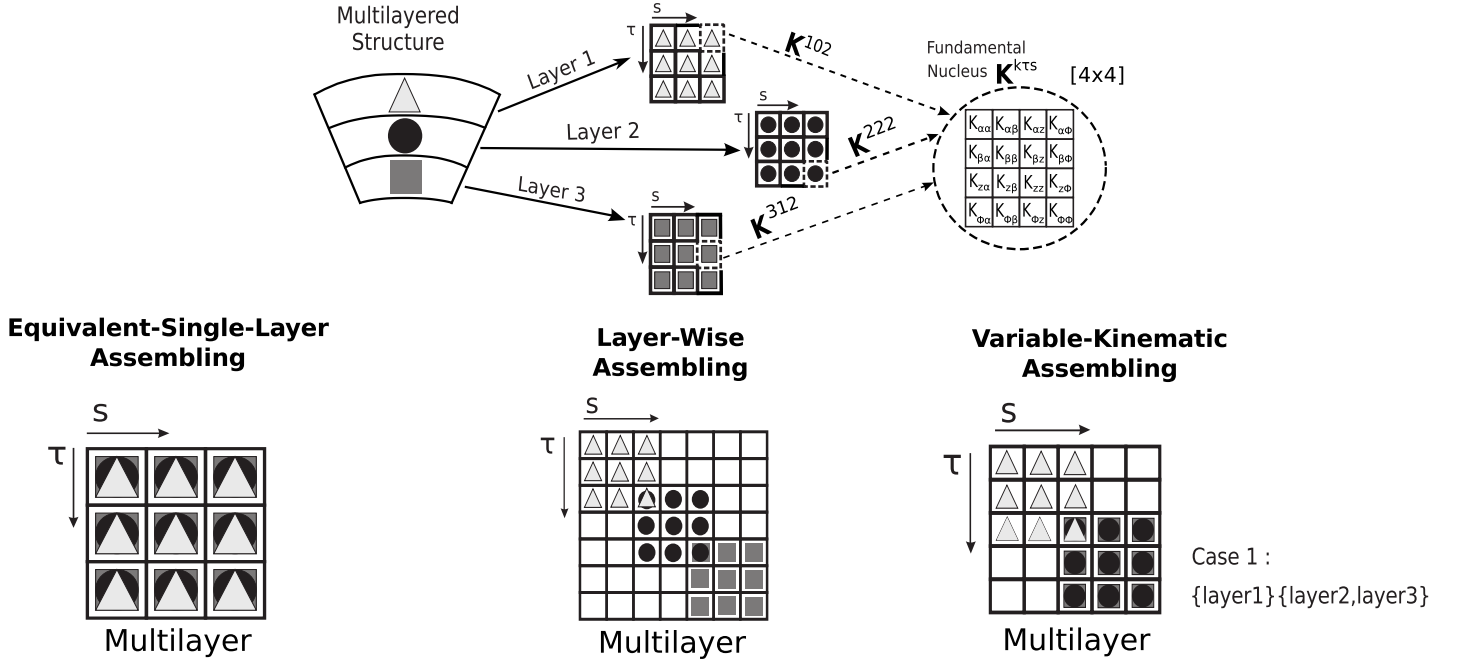


Figure 5: Overview of assembling scheme of the three different approaches.

Acronyms

Depending on the variables description and the number of terms N of the various expansion of kinematics plate theories can be obtained. A system of acronyms is given to denote these models. The first letters indicate the used approach in this work which is Equivalent Single Layer (E). The second letter indicates the type of polynomial adopted, (L) for the Legendre's polynomials. Sometimes a reference solution is given with a layer-wise approach, so the first letters become LW. The number N indicates the number of terms of the expansion used in the thickness direction. If the Navier analytical method is employed the subscript (a) is used. The letter Z is added if the zig-zag function of Murakami is employed.

7 Numerical results

To assess these theories the following reference problems have been considered:

- A four-layer square plate with a cross-ply composite core $[0^\circ/90^\circ]$ and piezoelectric external skins
- A three-layer cylindrical shell with a composite core and piezoelectric external skins
- A four-layer cylindrical shell with a cross-ply composite core $[90^\circ/0^\circ]$ and piezoelectric external skins

7.1 Four-layer plate

A four-layer cross-ply square plate, see Figure 6, with a cross-ply Gr/Ep composite core $[0^\circ/90^\circ]$ and PZT-4 piezoelectric external skins, simply-supported boundary condition is considered. The static analysis of the plate structure is evaluated in sensor and actuator configuration.

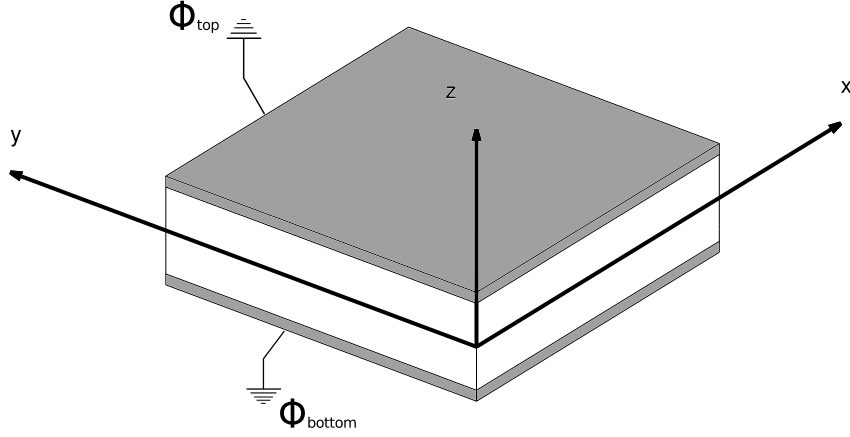


Figure 6: Reference system of the composite plate with piezoelectric skins.

For the sensor case, a bi-sinusoidal transverse normal pressure is applied to the top surface of the plate:

$$p(x, y, z_{top}) = p_z^o \sin(m\pi x/a) \sin(n\pi y/b) \quad (28)$$

with amplitude $p_z^o = 1$ and wave numbers $m = 1$, $n = 1$. The potential at top and bottom position is imposed $\Phi_t = \Phi_b = 0$.

For the actuator case, a bi-sinusoidal electric potential is imposed at top surface:

$$\Phi(x, y, z_{top}) = \phi_z^o \sin(m\pi x/a) \sin(n\pi y/b) \quad (29)$$

with amplitude $\phi_z^o = 1$ and wave numbers $m = 1$, $n = 1$. The potential at bottom position is imposed $\Phi_b = 0$. No mechanical load is applied.

In respect to the total thickness, a single piezoelectric skin is thick $h_p = 0.1h_{tot}$, while the single core layer is thick $h_c = 0.4h_{tot}$. The material properties of the plate are given in Table 1.

Table 1: Material data for multilayered plate and shell.

Properties	PZT-4	Gr/EP
E_{11} [GPa]	81.3	132.38
E_{22} [GPa]	81.3	10.756
E_{33} [GPa]	64.5	10.756
ν_{12} [-]	0.329	0.24
ν_{13} [-]	0.432	0.24
ν_{23} [-]	0.432	0.49
G_{12} [GPa]	30.6	5.6537
G_{13} [GPa]	25.6	5.6537
G_{23} [GPa]	25.6	3.606
e_{15} [C/m ²]	12.72	0
e_{24} [C/m ²]	12.72	0
e_{31} [C/m ²]	-5.20	0
e_{32} [C/m ²]	-5.20	0
e_{33} [C/m ²]	15.08	0
$\tilde{\epsilon}_{11}/\epsilon_0$ [-]	1475	3.5
$\tilde{\epsilon}_{22}/\epsilon_0$ [-]	1475	3.0
$\tilde{\epsilon}_{33}/\epsilon_0$ [-]	1300	3.0
ϵ_0 [C/Vm]	$8.85 * 10^{-12}$	$8.85 * 10^{-12}$

The results are calculated for different thickness ratios $a/h = 2, 100$, and they are evaluated in the following positions with the following form for the sensor cases:

$$\begin{aligned} \hat{w}(x, y, z) &= w(a/2, b/2, 0) * 10^{11} & , & \quad \hat{\sigma}_{xx}(x, y, z) = \sigma_{xx}(a/2, b/2, +h/2) \\ \hat{\sigma}_{xz}(x, y, z) &= \sigma_{xz}(a, b/2, 0) & , & \quad \hat{\sigma}_{zz}(x, y, z) = \sigma_{zz}(a/2, b/2, +h/2) \\ \hat{\Phi}(x, y, z) &= \Phi(a/2, b/2, 0) * 10^3 & , & \quad \hat{\mathcal{D}}_z(x, y, z) = \mathcal{D}_z(a/2, b/2, +h/2) * 10^9 \end{aligned}$$

For the actuator cases the variables are evaluated in the same way as the sensor cases, except for the electric potential:

$$\hat{\Phi}(x, y, z) = \Phi(a/2, b/2, 0)$$

First, a convergence study on the plate element was performed. A composite plate with thickness ratios $a/h = 100$ is evaluated. For the sensor case a mesh grid of 40×40 elements ensures the convergence of both the mechanical and electrical variables except for the transverse electric displacement \mathcal{D}_z that has a very slow convergence rate. For the actuator case a mesh grid of 24×24 elements ensures the convergence for all the variables, see Table 2.

Table 2: Convergence study. Composite four layered plate with thickness ratio $a/h = 100$.

Sensor Case												
Mesh	4 × 4	8 × 8	12 × 12	16 × 16	20 × 20	24 × 24	28 × 28	32 × 32	36 × 36	40 × 40	<i>Analytical</i> [Ballhause et al., 2005]	
LW4	\hat{w}	4678433	4675324	4675148	4675117	4675109	4675106	4675104	4675104	4675103	4675300	
	$\hat{\sigma}_{xx}$	3302.4	3182.6	3160.1	3152.3	3148.7	3146.7	3145.5	3144.7	3144.2	3142.1	
	$\hat{\sigma}_{xz}$	-20.154	-19.167	-18.975	-18.909	-18.879	-18.863	-18.854	-18.849	-18.845	-18.842	-18.832
	$\hat{\sigma}_{zz}$	18.210	2.306	1.284	1.101	1.047	1.025	1.015	1.009	1.006	1.003	-
	$\hat{\Phi}$	4780.7	4636.5	4605.7	4594.6	4589.5	4586.7	4585.1	4584.1	4583.5	4583.0	4580.2
	\hat{D}_z	-1.2691	-0.1006	-0.0307	-0.0193	-0.0165	-0.0154	-0.0149	-0.0144	-0.0140	-0.0136	0.0136
Actuator Case												
Mesh	4 × 4	8 × 8	12 × 12	16 × 16	20 × 20	24 × 24	<i>Analytical</i> [Ballhause et al., 2005]					
LW4	\hat{w}	-1.3486	-1.3492	-1.3493	-1.3493	-1.3493	-1.3493	-1.3493				
	$\hat{\sigma}_{xx}$	-0.0238	-0.0244	-0.0245	-0.0245	-0.0245	-0.0246	-0.0246				
	$\hat{\sigma}_{xz}$	0.0000	0.0000	0.0000	0.0000	0.0000	0.0000	0.0000				
	$\hat{\sigma}_{zz}$	0.0002	0.0000	0.0000	0.0000	0.0000	0.0000	-				
	$\hat{\Phi}$	0.4999	0.4999	0.4999	0.4999	0.4999	0.4999	0.4999				
	\hat{D}_z	-0.0370	-0.0370	-0.0370	-0.0370	-0.0370	-0.0370	-0.0370				

Therefore a locking study has been performed evaluating different types of integration methods [Hughes et al., 1978] for the same plate structure to prove that the element is locking free, see Table 3. The plate element with the MITC9 method ensures accuracy on both the transverse displacement and the shear stress.

Table 3: Locking study. Composite four layered plate with thickness ratio $a/h = 100$. The Sensor cases are computed with a mesh of 40×40 elements, the Actuator cases are computed with a mesh of 24×24 elements.

Sensor Case					Actuator Case				
	<i>Reduced</i>	<i>Selective</i>	<i>MITC9</i>	<i>Analytical</i> [Ballhause et al., 2005]	<i>Reduced</i>	<i>Selective</i>	<i>MITC9</i>	<i>Analytical</i> [Ballhause et al., 2005]	
LW4	\hat{w}	4675103	4675003	4675103	4675300	-1.3493	-1.3496	-1.3493	-1.3493
	$\hat{\sigma}_{xz}$	-23.096	-22.018	-18.842	-18.832	0.0000	0.0000	0.0000	0.0000
	$\hat{\Phi}$	4581.9	4582.7	4583.0	4580.2	0.4999	0.4999	0.4999	0.4999
	\hat{D}_z	-0.1511	0.0340	-0.0136	0.0136	-0.0366	-0.0370	-0.0370	-0.0370

An assessment of the Legendre polynomials with a full ESL approach has been performed for the pure mechanical case in [Pagani et al.,] for plates and in [Carrera et al., 2017] for shells. All the results presented in [Pagani et al., , Carrera et al., 2017], for thick and thin plates and shells, show that the Legendre polynomials lead to the same results of the Taylor polynomials. The use of either polynomial is invariant respect to the solution accuracy.

Hereafter Legendre polynomials have been employed for the structure analyzes. Different Variable Kinematic models have been used to perform the analysis of the plate structures, see Figures 7. The acronyms have been modified adding a subscript to them, for the sake of clarity the list of subscripts is given below:

- $Case1 = \{layer1\} \{layer2, layer3, layer4\}$
- $Case2 = \{layer1, layer2, layer3\} \{layer4\}$
- $Case3 = \{layer1\} \{layer2, layer3\} \{layer4\}$

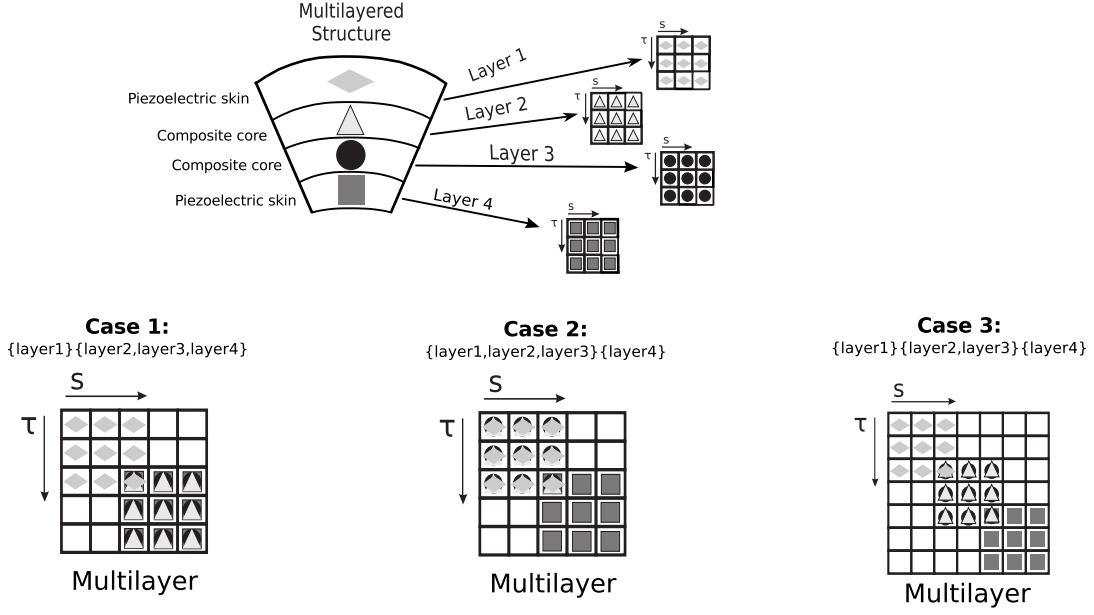


Figure 7: Variable Kinematic Cases. Compact example of assembling scheme.

The results are listed in Table 4 for the sensor case, and in Table 5 for the actuator case. For the plate structures analysed the following considerations can be drawn for the sensor cases:

- Regarding the transverse displacement w , for thin plates $a/h = 100$, the theories $EL4_{,Case1}$, $EL4_{,Case2}$ and $EL4_{,Case3}$ lead an improvement of the solution respect to the $EL4$ without appreciable differences within them, see Figure 8a. For thick plates $a/h = 2$, the variable kinematic theories show different levels of accuracy. The $EL4_{,Case3}$ theory is able to approximate very well the full layer-wise reference solution $LW4$. It has to be noticed that the $EL4_{,Case1}$ theory has a better behaviour than the $EL4_{,Case2}$ theory due to the layer-wise approximation of the upper loaded layer, see Figure 8b.
- For both the transverse shear stress σ_{xz} , see Figure 9a, and the transverse normal stress, see Figure 9b, the theories $EL4_{,Case1}$ and $EL4_{,Case2}$ improve the results respect to the $EL4$ theory only in the layer with a layer-wise description. The $EL4_{,Case3}$ theory is able to approximate very well along the entire thickness of the plate the full layer-wise reference solution $LW4$.
- Regarding the electric potential Φ , for thin plates $a/h = 100$, the theories $EL4_{,Case1}$, $EL4_{,Case2}$ and $EL4$ theories overestimate the reference solution, see Figure 10a. For thick plates $a/h = 2$, the variable kinematic theories can underestimate and overestimate the solution, see Figure 10b. For both thin and thick plates only the $EL4_{,Case3}$ theory is able to approximate very well the full layer-wise reference solution $LW4$.
- For the electric transverse displacement D_z , for both thin plates $a/h = 100$, see Figures 11a, and thick plates $a/h = 2$, see Figures 11b, the theories $EL4_{,Case1}$ and $EL4_{,Case2}$ improve the results respect to the $EL4$ theory only in the layer with a layer-wise description. The $EL4_{,Case3}$ theory is the best approximating theory respect to the full layer-wise reference solution $LW4$.

For the plate structures analysed in actuator configuration, the following considerations can be drawn:

- Regarding the transverse displacement w , for thin plates $a/h = 100$, the variable kinematic theories show different levels of accuracy, see Figure 12a, the $EL4_{,Case3}$ solution is closer than $EL4_{,Case1}$ and $EL4_{,Case2}$ theories to the full layer-wise reference solution $LW4$. For thick plates

$a/h = 2$ the $EL4,Case1$ and $EL4,Case3$ theories are able to approximate very well the full layer-wise reference solution $LW4$, see Figure 12b.

- For both the transverse shear stress σ_{xz} , see Figure 13a, and the transverse normal stress, see Figure 13b, the same considerations as the sensor cases can be depicted. The theories $EL4,Case1$ and $EL4,Case2$ improve the results respect to the $EL4$ theory only in the layer with a layer-wise description. The $EL4,Case3$ theory is able to approximate very well along the entire thickness of the plate the full layer-wise reference solution $LW4$.
- Regarding the electric potential Φ , for thin plates $a/h = 100$, see Figure 14a, the theories $EL4,Case1$, $EL4,Case2$ and $EL4$ theories can underestimate and overestimate the solution in the central composite layers. The $EL4,Case3$ theory is able to approximate very well the full layer-wise reference solution $LW4$.
- For the electric transverse displacement \mathcal{D}_z , for thick plates $a/h = 2$, see Figures 14b, the theories $EL4,Case1$ and $EL4,Case2$ improve the results respect to the $EL4$ theory only in the layer with a layer-wise description. The $EL4,Case3$ theory is the best approximating theory respect to the full layer-wise reference solution $LW4$.

Therefore, the euclidean norm of the error of primary variables (mechanical displacements, and electric potential), and secondary variables (mechanical stresses, and electric displacements), is evaluated along the plate thickness by mono-models and variable-kinematic models, respect to the adopted reference solution $ref = LW4$. The euclidean norm of the error $\|f_E\|_2$ is calculated for a generic mechanical or electric variables f along the plate thickness z as follows:

$$\|f_E\|_2 = \sqrt{\int_{z_1}^{z_2} (f_{ref}(z) - f(z))^2 dz} \quad (30)$$

for a multilayered structure, the integral is splitted, along the thickness direction z , in the integral sum of each layer k . Equation 30 changes into:

$$\|f_E\|_2 = \sqrt{\sum_{k=1}^{N_{layers}} \int_{z_1^k}^{z_2^k} (f_{ref}^k(z) - f^k(z))^2 dz^k} \quad (31)$$

The euclidean norms are listed in Table 6 for various aspect ratios, and both sensor and actuator case are taken into account. Here, the norm is a global indicator of the solution accuracy along the multilayer thickness, it is not distinguishing the local layer approximation. For the Sensor case (mechanical load applied), the mechanical variables have almost the same solution accuracy independently of the used kinematic model. The variable-kinematic model *Case 3*, where the piezoelectric skins have to be modeled by a layer-wise description, permits to have an huge reduction of the error ($10^3 : 10^4$ times) respect to the others mono-models and variable-kinematic models, for the description of the electric potential Φ , and for the electric transverse displacement \mathcal{D}_z . For the Actuator case (electrical load applied), the variable-kinematic model *Case 3*, where the piezoelectric skins have to be modeled by a layer-wise description, permits to have better results for both mechanical and electrical variables. The mechanical variables show an error reduction of ($10^3 : 10^5$ times) respect to the other kinematic models. The accuracy of the electric variables is improved more than mechanical ones, the error is ($10^3 : 10^8$ times) lower than the other kinematic models.

For the multilayered plate structures, in conclusion, it is clear that to have more accurate results, the piezoelectric skins have to be modeled by a layer-wise description. The Variable-Kinematic model permits to improve globally the results, and at the same time permits to reduce the computational cost of the analysis, assembling the composite core with an equivalent-single-layer model.

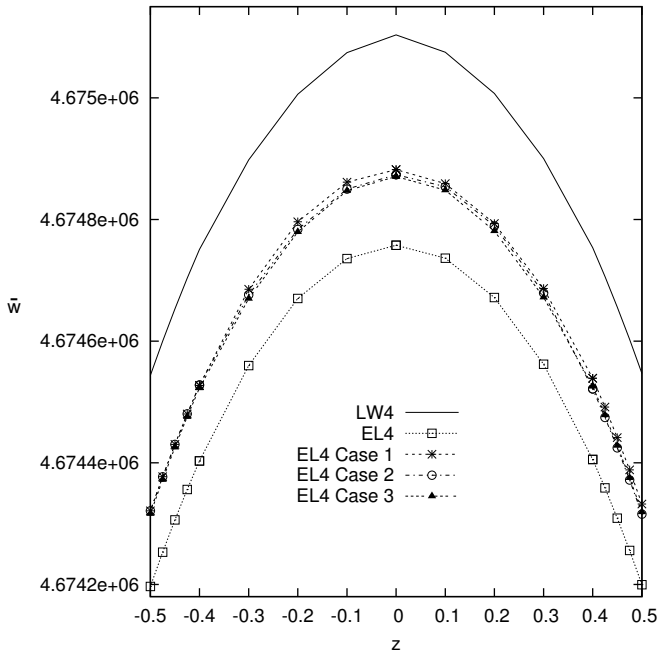
Table 4: Four-layer square plate with a cross-ply composite core $[0^\circ/90^\circ]$ and piezoelectric external skins. Mechanical and electrical variables described by Mono-models and Variable kinematic models for various aspect ratios a/h . Sensor case.

	$a/h = 100$						$DOFs$
	\hat{w}	$\hat{\sigma}_{xx}$	$\hat{\sigma}_{xz}$	$\hat{\sigma}_{zz}$	$\hat{\Phi}$	\hat{D}_z	
$LW4_a$ [Ballhause et al., 2005]	4675300	3142.1	-18.832	-	4580.2	0.0136	
<i>LW4</i>	4675103	3143.8	-18.842	1.004	4583.0	-0.0136	446148
<i>LW1</i>	4647068	3268.7	-18.909	342.0	4555.3	-23.863	131220
<i>EL3Z</i>	4674435	3142.2	-26.188	43.85	6967.9	-21.051	131220
<i>EL4</i>	4674758	3133.9	-27.238	-37.15	12122	7.9569	131220
<i>EL3</i>	4674453	3153.0	-26.719	23.08	12658	-1.5890	104976
<i>EL2</i>	4669551	3152.5	-10.677	23.56	12660	-1.0612	78732
<i>EL1</i>	3719168	3657.9	-10.203	2727	0.0000	-190.38	52488
<i>EL4_{Case1}</i>	4674882	3143.9	-25.668	1.004	9320.7	0.2112	236196
<i>EL4_{Case2}</i>	4674874	3141.3	-25.386	-19.59	9308.7	6.5076	236196
<i>EL4_{Case3}</i>	4674870	3143.8	-24.713	1.004	4582.9	-0.0135	341172
<i>EL3_{Case1}</i>	4674914	3144.0	-26.972	1.004	10412	0.3304	183708
<i>EL3_{Case2}</i>	4674905	3151.0	-25.839	-38.11	10396	23.176	183708
<i>EL3_{Case3}</i>	4674740	3143.8	-24.463	1.004	4582.8	-0.0135	262440
<i>EL2_{Case1}</i>	4673789	3143.2	-17.418	1.029	12620	0.3017	131220
<i>EL2_{Case2}</i>	4673770	3159.6	-21.524	38.19	12613	-2.8657	131220
<i>EL2_{Case3}</i>	4674702	3143.8	-23.057	1.029	4582.7	-0.0139	183708
<i>EL1_{Case1}</i>	4405952	3105.1	-14.014	324.3	2521.9	14.873	78732
<i>EL1_{Case2}</i>	4405007	3483.4	-14.290	1742	2522.2	-360.17	78732
<i>EL1_{Case3}</i>	4560604	3214.1	-22.118	335.6	4472.9	-23.419	104976

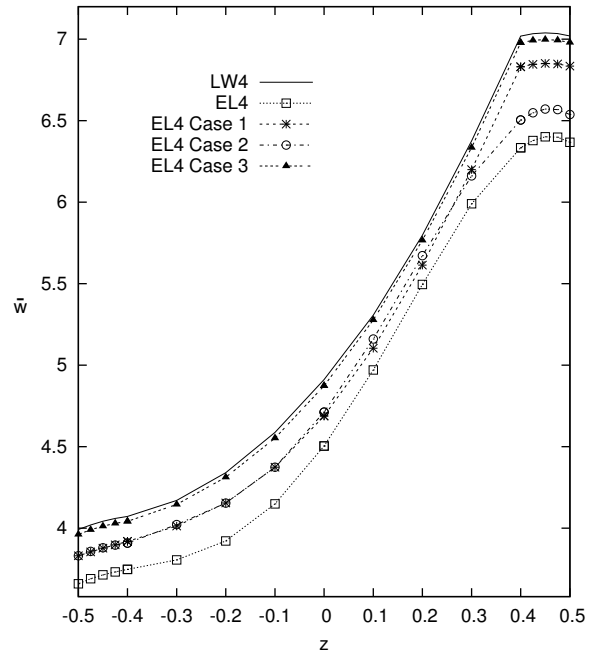
	$a/h = 2$						$DOFs$
	\hat{w}	$\hat{\sigma}_{xx}$	$\hat{\sigma}_{xz}$	$\hat{\sigma}_{zz}$	$\hat{\Phi}$	\hat{D}_z	
$LW4_a$ [Ballhause et al., 2005]	4.9113	3.2207	-0.26995	-	0.9103	0.0256	
<i>LW4</i>	4.9112	3.2220	-0.27556	1.0002	0.9106	0.0257	446148
<i>LW1</i>	4.8087	3.5198	-0.31619	2.1220	0.8600	-0.0663	131220
<i>EL3Z</i>	4.3973	3.3894	-0.45298	1.5681	23.803	-0.0579	131220
<i>EL4</i>	4.5038	2.3684	-0.46102	-0.3149	-6.0143	-0.0938	131220
<i>EL3</i>	4.6282	3.1386	-0.45210	1.6818	2.9967	-0.1295	104976
<i>EL2</i>	2.9334	2.3985	-0.19243	2.1722	4.1979	0.3281	78732
<i>EL1</i>	2.8907	2.1141	-0.19247	2.4231	0.0000	0.1730	52488
<i>EL4_{Case1}</i>	4.6885	3.1302	-0.42763	1.0002	2.4015	0.0252	236196
<i>EL4_{Case2}</i>	4.7123	2.4890	-0.40574	-0.4832	-9.0305	0.0531	236196
<i>EL4_{Case3}</i>	4.8731	3.2003	-0.40012	1.0002	0.9037	0.0256	341172
<i>EL3_{Case1}</i>	4.6374	3.1506	-0.45238	1.0048	4.1069	0.0255	183708
<i>EL3_{Case2}</i>	4.6556	3.0310	-0.44481	0.8657	-10.643	-0.0182	183708
<i>EL3_{Case3}</i>	4.8779	3.1923	-0.40117	1.0050	0.9049	0.0258	262440
<i>EL2_{Case1}</i>	4.1357	2.5720	-0.30963	1.0249	6.9886	0.0227	131220
<i>EL2_{Case2}</i>	4.1730	3.0466	-0.32652	2.2611	1.8004	0.0260	131220
<i>EL2_{Case3}</i>	4.8895	3.1797	-0.39916	1.0325	0.8674	0.0272	183708
<i>EL1_{Case1}</i>	4.2378	3.1781	-0.29120	1.8672	0.8329	0.0204	78732
<i>EL1_{Case2}</i>	3.2987	1.8259	-0.24482	2.0088	1.0888	0.1602	78732
<i>EL1_{Case3}</i>	5.0470	3.2388	-0.40237	2.0573	1.4450	-0.0620	104976

Table 5: Four-layer square plate with a cross-ply composite core $[0^\circ/90^\circ]$ and piezoelectric external skins. Mechanical and electrical variables described by Mono-models and Variable kinematic models for various aspect ratios a/h . Actuator case.

	$a/h = 100$						$DOFs$
	\hat{w}	$\hat{\sigma}_{xx}$	$\hat{\sigma}_{xz}$	$\hat{\sigma}_{zz}$	$\hat{\Phi}$	\hat{D}_z	
$LW4_a$ [Ballhause et al., 2005]	-1.3493	-0.0246	0.0000	-	0.4999	-0.0370	
<i>LW4</i>	-1.3493	-0.0246	0.0000	0.0000	0.4999	-0.0370	163268
<i>LW1</i>	-1.3970	-0.0210	0.0000	0.0035	0.4999	-0.0353	48020
<i>EL3Z</i>	-3.6123	1.8546	-0.0154	-4.8765	0.4969	3.7228	48020
<i>EL4</i>	-3.2153	1.8587	-0.0087	-4.8932	0.5000	3.7332	48020
<i>EL3</i>	-3.1556	1.8607	-0.0117	-4.8929	0.5000	3.7340	38416
<i>EL2</i>	-13.288	-8.2308	0.0186	5.4440	0.5000	-13.546	28812
<i>EL1</i>	-14.415	-8.2361	0.0198	5.4391	0.5000	-13.544	19208
<i>EL4_{Case 1}</i>	-23.806	-0.0362	-0.0002	0.0000	0.3220	-0.0452	86436
<i>EL4_{Case 2}</i>	19.359	0.0934	-0.0046	-0.0148	0.6780	0.0516	86436
<i>EL4_{Case 3}</i>	-1.3493	-0.0246	0.0000	0.0000	0.4999	-0.0370	124852
<i>EL3_{Case 1}</i>	35.698	-0.0417	-0.0002	0.0000	0.2554	-0.0525	67228
<i>EL3_{Case 2}</i>	30.710	0.5397	-0.0140	-1.4381	0.7445	1.0801	67228
<i>EL3_{Case 3}</i>	-1.3492	-0.0246	0.0000	0.0000	0.4999	-0.0370	96040
<i>EL2_{Case 1}</i>	-32.853	-0.0398	-0.0001	0.0000	0.2810	-0.0529	48020
<i>EL2_{Case 2}</i>	23.714	0.6197	0.0102	-1.9831	0.7190	1.3987	48020
<i>EL2_{Case 3}</i>	-1.3492	-0.0246	0.0000	0.0000	0.4999	-0.0370	67228
<i>EL1_{Case 1}</i>	-3744.8	-2.0834	-0.0001	-0.2717	0.5487	-1.6144	28812
<i>EL1_{Case 2}</i>	3725.0	-6.0577	0.0262	10.138	0.4513	-14.470	28812
<i>EL1_{Case 3}</i>	-1.3711	-0.0210	0.0000	0.0035	0.5000	-0.0353	38416
	$a/h = 2$						$DOFs$
	\hat{w}	$\hat{\sigma}_{xx}$	$\hat{\sigma}_{xz}$	$\hat{\sigma}_{zz}$	$\hat{\Phi}$	\hat{D}_z	
$LW4_a$ [Ballhause et al., 2005]	-1.7475	3.8162	0.0864	-	0.3330	-9.4085	
<i>LW4</i>	-1.7475	3.8329	0.0928	0.0006	0.3330	-9.4093	163268
<i>LW1</i>	-2.1030	12.452	0.0215	8.1858	0.3241	-5.2964	48020
<i>EL3Z</i>	-1.4360	5.9403	-0.4065	10.264	-1.5893	-8.2244	48020
<i>EL4</i>	-4.4070	10.954	-0.1212	-0.2279	0.5118	-4.0866	48020
<i>EL3</i>	-4.0468	13.687	-0.1547	-0.5378	0.4615	-2.0398	38416
<i>EL2</i>	-12.428	-3.0088	1.0887	7.3130	0.4674	-16.882	28812
<i>EL1</i>	-14.415	-11.286	1.1108	0.6048	0.5000	-14.549	19208
<i>EL4_{Case 1}</i>	-1.6859	3.8635	0.1467	0.0006	0.2387	-9.4124	86436
<i>EL4_{Case 2}</i>	-4.2234	8.0541	0.0733	4.8358	0.6467	-8.9133	86436
<i>EL4_{Case 3}</i>	-1.7323	3.8406	0.1339	0.0006	0.3330	-9.4092	124852
<i>EL3_{Case 1}</i>	-1.7082	3.8931	0.1402	0.0269	0.2076	-9.4088	67228
<i>EL3_{Case 2}</i>	-5.3533	10.947	-0.4043	4.5420	0.7964	-6.1619	67228
<i>EL3_{Case 3}</i>	-1.7510	3.8810	0.1413	0.0268	0.3310	-9.4034	96040
<i>EL2_{Case 1}</i>	-1.2439	4.4452	0.0248	0.0604	0.2687	-9.3855	48020
<i>EL2_{Case 2}</i>	-10.423	7.5934	1.0047	-0.9364	0.6714	-3.6157	48020
<i>EL2_{Case 3}</i>	-1.7733	4.0563	0.0847	0.0549	0.3311	-9.3809	67228
<i>EL1_{Case 1}</i>	-5.3835	8.8014	0.2170	6.9842	0.5340	-6.7681	28812
<i>EL1_{Case 2}</i>	-13.537	-7.9884	1.3111	5.4393	0.4493	-15.734	28812
<i>EL1_{Case 3}</i>	-2.0311	12.943	0.1103	8.1694	0.4858	-5.2979	38416

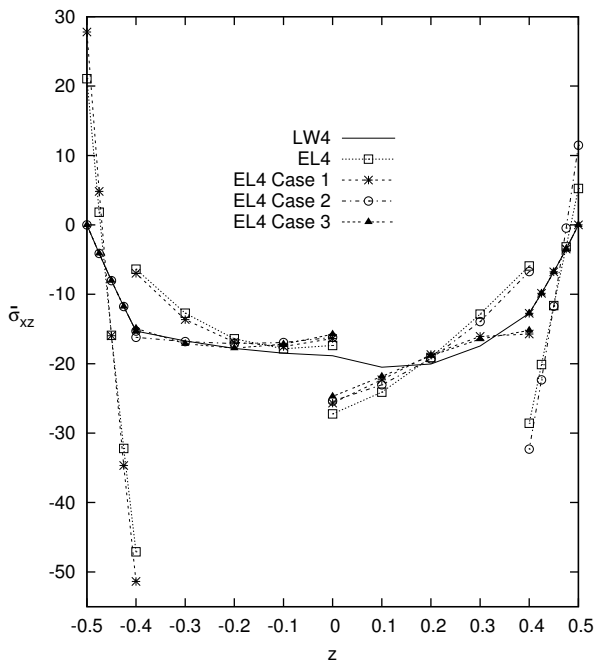


(a)

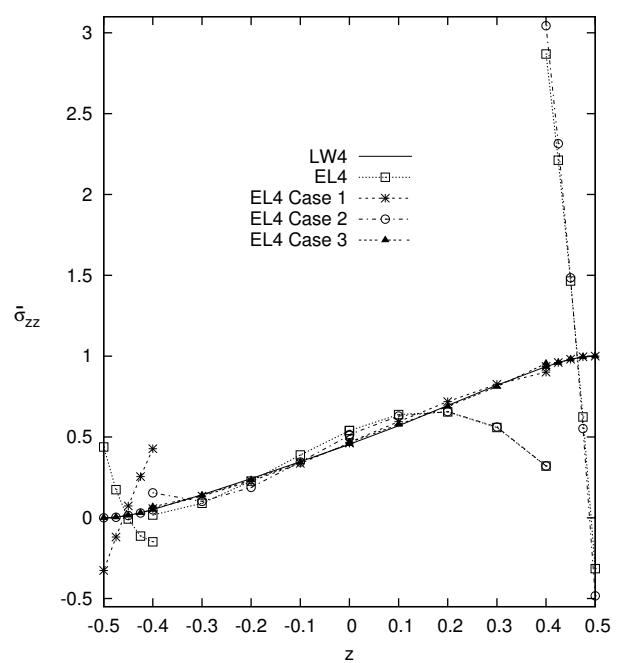


(b)

Figure 8: Four-layered plate, Sensor case, transverse mechanical displacement \hat{w} , $a/h = 100$ (a), $a/h = 2$ (b).

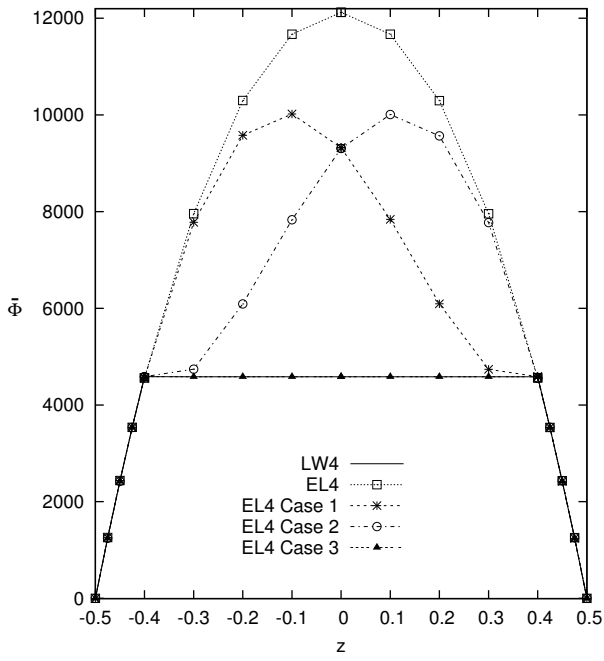


(a)

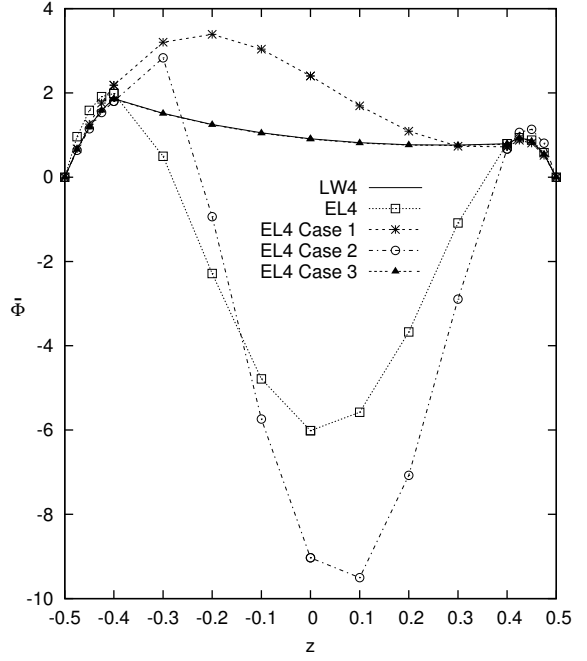


(b)

Figure 9: Four-layered plate, Sensor case, transverse mechanical stresses, $\hat{\sigma}_{xz}$ for $a/h = 100$ ratio (a), $\hat{\sigma}_{zz}$ for $a/h = 2$ ratio (b).

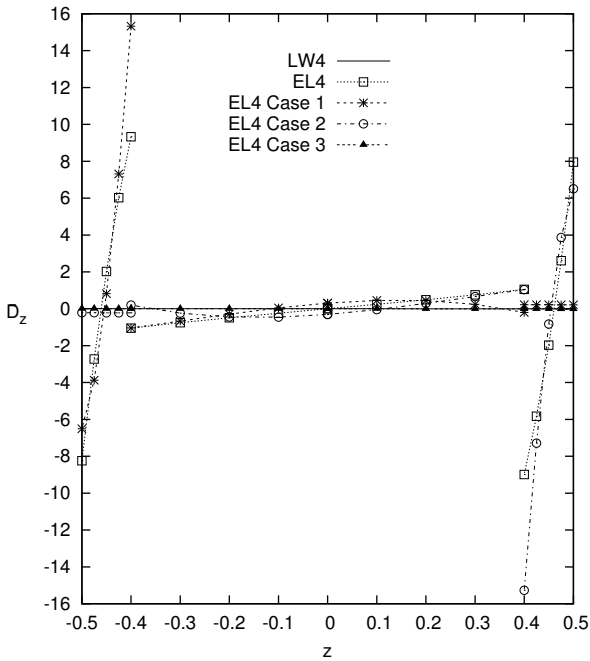


(a)

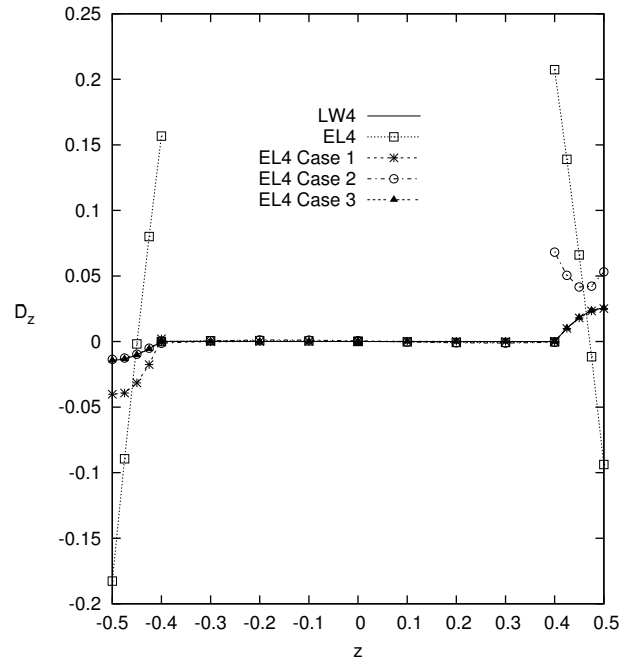


(b)

Figure 10: Four-layered plate, Sensor case, Electric Potential $\hat{\Phi}$, $a/h = 100$ (a), $a/h = 2$ (b).



(a)



(b)

Figure 11: Four-layered plate, Sensor case, transverse electric displacement \hat{D}_z , $a/h = 100$ (a), $a/h = 2$ (b).

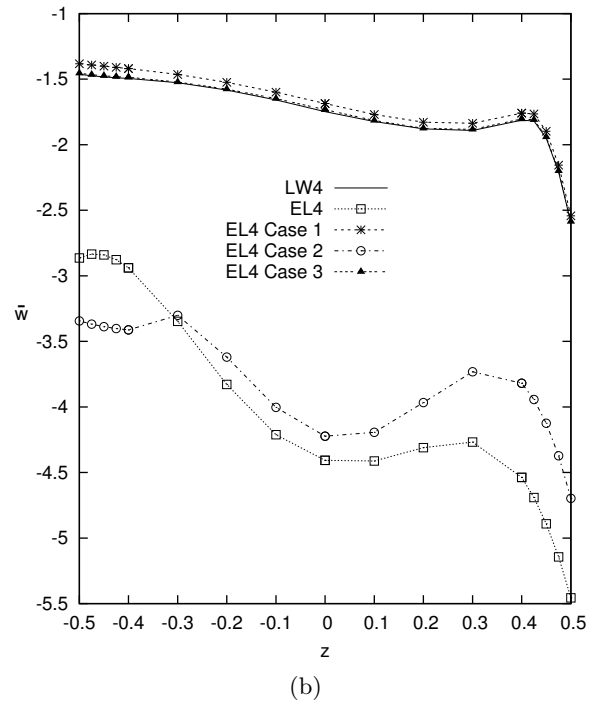
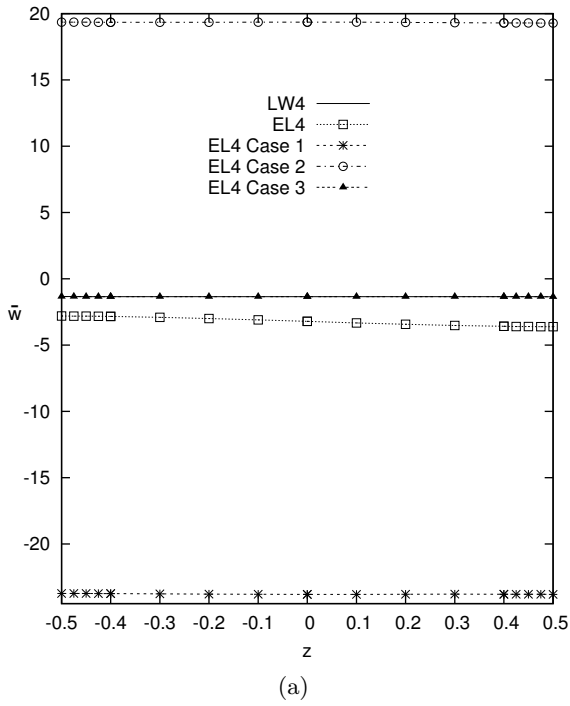


Figure 12: Four-layered plate, Actuator case, transverse mechanical displacement \hat{w} , $a/h = 100$ (a), $a/h = 2$ (b).

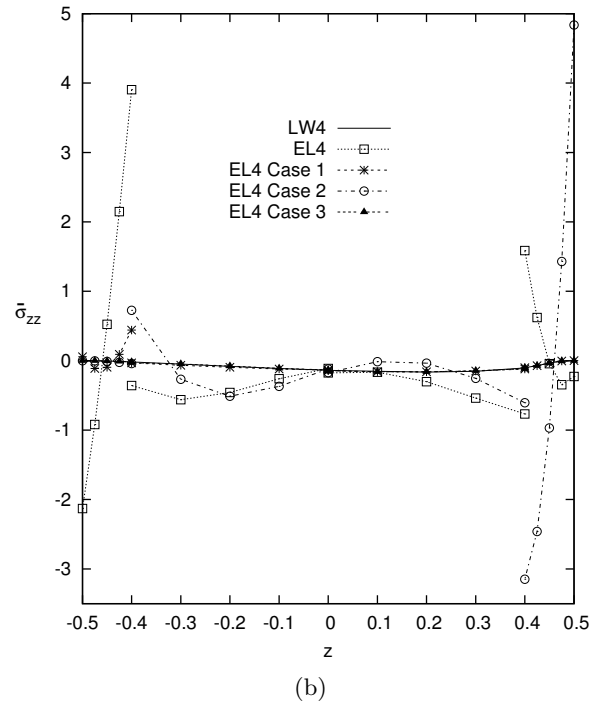
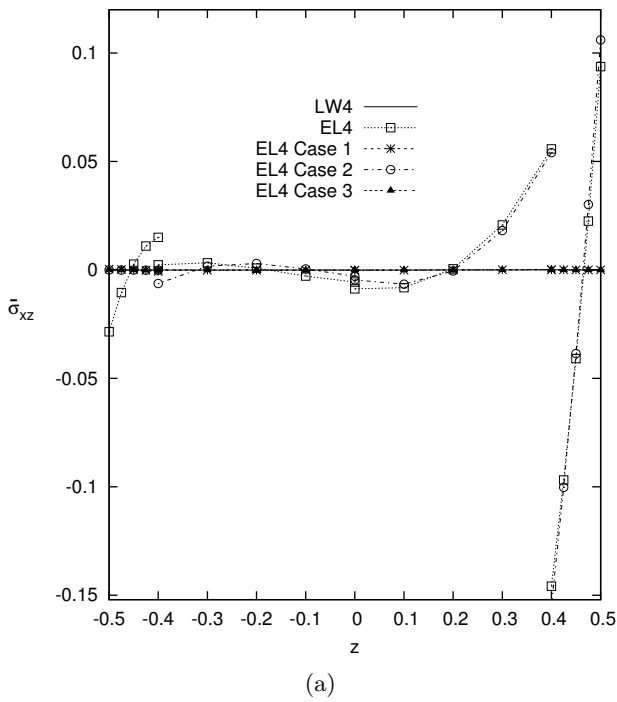


Figure 13: Four-layered plate, Actuator case, transverse mechanical stresses, $\hat{\sigma}_{xz}$ for $a/h = 100$ ratio (a), $\hat{\sigma}_{zz}$ for $a/h = 2$ ratio (b).

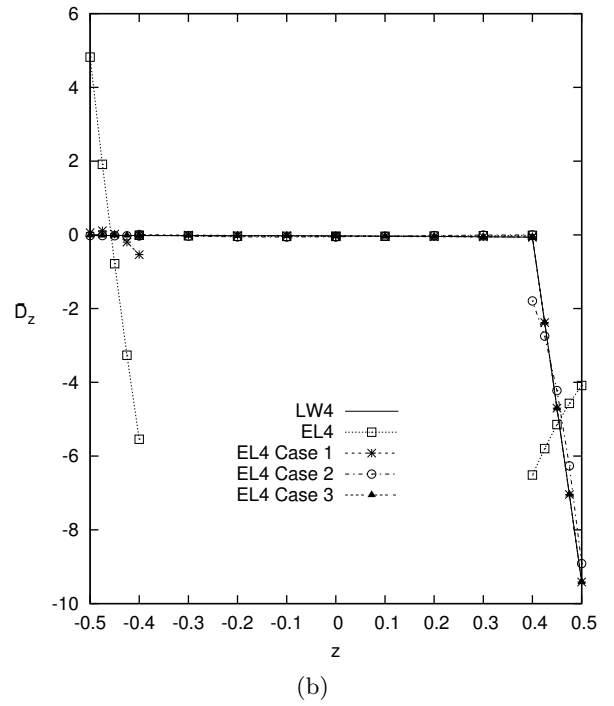
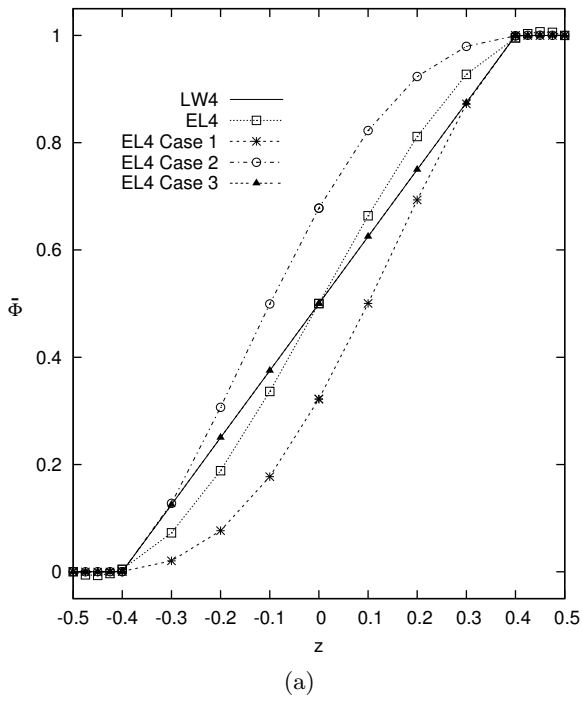


Figure 14: Four-layered plate, Actuator case, electric potential and electric transverse displacement, $\hat{\Phi}$ for $a/h = 100$ ratio (a), \hat{D}_z for $a/h = 2$ ratio (b).

Table 6: Four-layer square plate with a cross-ply composite core $[0^\circ/90^\circ]$ and piezoelectric external skins. Euclidean norm of the error respect to the reference solution *LW4* for mechanical and electrical variables described by Mono-models and Variable kinematic models for various aspect ratios a/h . Sensor and Actuator cases.

<i>Sensor Case</i>							
a/h		\hat{w}	$\hat{\Phi}$	$\hat{\sigma}_{xx}$	$\hat{\sigma}_{xz}$	$\hat{\sigma}_{zz}$	\hat{D}_z
100	<i>ELA</i>	0.3410 E+03	0.4954 E+04	0.5481 E+01	0.6929 E+01	0.1552 E+02	0.2390 E+01
	<i>ELACase1</i>	0.2155 E+03	0.3164 E+04	0.3934 E+01	0.6697 E+01	0.1039 E+02	0.2182 E+01
	<i>ELACase2</i>	0.2238 E+03	0.3157 E+04	0.3399 E+01	0.3995 E+01	0.1078 E+02	0.2177 E+01
	<i>ELACase3</i>	0.2278 E+03	0.1310 E+00	0.1955 E+01	0.1513 E+01	0.4410 E+01	0.2100 E-04
2	<i>ELA</i>	0.4228 E+00	0.3996 E+01	0.2865 E+00	0.1367 E+00	0.3652 E+00	0.4461 E-01
	<i>ELACase1</i>	0.1870 E+00	0.1211 E+01	0.7011 E-01	0.1131 E+00	0.6709 E-01	0.6323 E-02
	<i>ELACase2</i>	0.2424 E+00	0.5773 E+01	0.2423 E+00	0.1136 E+00	0.3874 E+00	0.1095 E-01
	<i>ELACase3</i>	0.3376 E-01	0.7868 E-02	0.4050 E-01	0.2977 E-01	0.6621 E-02	0.2712 E-04
<i>Actuator Case</i>							
a/h		\hat{w}	$\hat{\Phi}$	$\hat{\sigma}_{xx}$	$\hat{\sigma}_{xz}$	$\hat{\sigma}_{zz}$	\hat{D}_z
100	<i>ELA</i>	0.1886 E+01	0.4020 E-01	0.5294 E+00	0.2824 E-01	0.1361 E+01	0.1099 E+01
	<i>ELACase1</i>	0.2244 E+02	0.1142 E+00	0.5039 E-01	0.1077 E-03	0.9711 E-01	0.8997 E-01
	<i>ELACase2</i>	0.2069 E+02	0.1143 E+00	0.4999 E-01	0.2882 E-01	0.9694 E-01	0.9004 E-01
	<i>ELACase3</i>	0.4251 E-04	0.1880 E-08	0.5106 E-06	0.3669 E-05	0.1276 E-05	0.6322 E-08
2	<i>ELA</i>	0.2345 E+01	0.1261 E+00	0.1669 E+01	0.1458 E+01	0.6965 E+00	0.1454 E+01
	<i>ELACase1</i>	0.6071 E-01	0.6160 E-01	0.5113 E-01	0.3643 E-01	0.5155 E-01	0.6265 E-01
	<i>ELACase2</i>	0.2097 E+01	0.2057 E+00	0.1147 E+01	0.1469 E+01	0.7718 E+00	0.2346 E+00
	<i>ELACase3</i>	0.8899 E-02	0.1470 E-03	0.2288 E-01	0.1462 E-01	0.4666 E-02	0.6206 E-04

7.2 Three-layer cylindrical shell

A three-layer composite cylindrical shell, see Figure 15, with a Gr/Ep composite core and PZT-4 piezoelectric external skins, simply-supported boundary condition is considered. The static analysis of the shell structure is evaluated in sensor and actuator configuration.

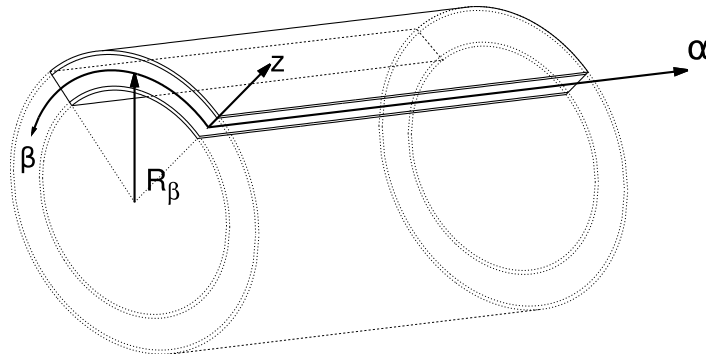


Figure 15: Reference system of the composite cylinder with piezoelectric skins.

For the sensor case a mechanical load pressure is applied, for the whole cylinder, at the inner surface

of the shell, defined as follows:

$$p(\alpha, \beta, z_{bottom}) = p^o \sin\left(\frac{m\pi\alpha}{a}\right) \cos\left(\frac{n\pi\beta}{b}\right) \quad (32)$$

with amplitude $p^o = 1$ and wave numbers $m = 1$ and $n = 8$. The potential at top and bottom position is imposed $\Phi_t = \Phi_b = 0$.

For the actuator case a bi-sinusoidal electric potential, for the whole cylinder, is imposed at outer surface:

$$\Phi(\alpha, \beta, z_{top}) = \phi^o \sin\left(\frac{m\pi\alpha}{a}\right) \cos\left(\frac{n\pi\beta}{b}\right) \quad (33)$$

with amplitude $\phi^o = 1$ and wave numbers $m = 1$, $n = 8$. The potential at bottom position is imposed $\Phi_b = 0$. No mechanical load is applied.

The material properties of the cylinder are given in Table 1. For all the cases the geometrical data are $a = 40$, $b = 2\pi R_\beta$, $R_\beta = 10$. In respect to the total thickness, a single piezoelectric skin is thick $h_p = 0.1h_{tot}$, while the single core layer is thick $h_c = 0.8h_{tot}$. The results are presented for different radius to thickness ratios $R_\beta/h = 2, 4, 10, 100$. Due to the geometrical symmetry of the cylinder, the symmetry of the load pressure and boundary condition, and the symmetry of the lamination stacking sequence, an octave of the cylinder is analyzed, half cylinder along the α axis direction and a quarter along the β circumferential axis direction. The applied mechanical load for an octave of the cylinder is defined as follows:

$$p(\alpha, \beta, z_{bottom}) = p^o \cos\left(\frac{m\pi\alpha}{a}\right) \cos\left(\frac{n\pi\beta}{b}\right) \quad (34)$$

and the electric load for an octave of the cylinder is defined as follows:

$$\Phi(\alpha, \beta, z_{top}) = \phi^o \cos\left(\frac{m\pi\alpha}{a}\right) \cos\left(\frac{n\pi\beta}{b}\right) \quad (35)$$

where $m = 0, 5$ and $n = 2$. The results are calculated in the following positions with the following form for the sensor cases:

$$\begin{aligned} \hat{w}(\alpha, \beta, z) &= w(a/2, 0, 0) * 10^{11} & , & \quad \hat{\sigma}_{\alpha\alpha}(\alpha, \beta, z) = \sigma_{\alpha\alpha}(a/2, 0, +h/2) \\ \hat{\sigma}_{\alpha z}(\alpha, \beta, z) &= \sigma_{\alpha z}(a, 0, 0) & , & \quad \hat{\sigma}_{zz}(\alpha, \beta, z) = \sigma_{zz}(a/2, 0, 0) \\ \hat{\Phi}(\alpha, \beta, z) &= \Phi(a/2, 0, 0) & , & \quad \hat{\mathcal{D}}_z(\alpha, \beta, z) = \mathcal{D}_z(a/2, 0, +h/2) * 10^{11} \end{aligned}$$

For the actuator cases the variables are evaluated in the following form:

$$\begin{aligned} \hat{w}(\alpha, \beta, z) &= w(a/2, 0, 0) * 10^{11} & , & \quad \hat{\sigma}_{\alpha\alpha}(\alpha, \beta, z) = \sigma_{\alpha\alpha}(a/2, 0, +h/2) \\ \hat{\sigma}_{\alpha z}(\alpha, \beta, z) &= \sigma_{\alpha z}(a, 0, 0) * 10^4 & , & \quad \hat{\sigma}_{zz}(\alpha, \beta, z) = \sigma_{zz}(a/2, 0, 0) * 10^4 \\ \hat{\Phi}(\alpha, \beta, z) &= \Phi(a/2, 0, 0) & , & \quad \hat{\mathcal{D}}_z(\alpha, \beta, z) = \mathcal{D}_z(a/2, 0, +h/2) * 10^{11} \end{aligned}$$

First a convergence study on the shell element was performed. A composite shell with radius to thickness ratio $R_\beta/h = 100$ is evaluated. For the sensor case a mesh grid of 20×80 elements ensures the convergence of both the mechanical and electrical variables except for the transverse electric displacement \mathcal{D}_z that has a very slow convergence rate. For the actuator case a mesh grid of 14×56 elements ensures the convergence for all the variables, see Table 7.

Table 7: Convergence study. Composite three layered cylindrical shell with radius to thickness ratio $R_\beta/h = 100$.

		Sensor Case										
	Mesh	2×8	4×16	6×24	8×32	10×40	12×48	14×56	16×64	18×72	20×80	<i>Analytical</i> [Cinefra et al., 2015a]
LW4	\hat{w}	403698	403225	403194	403188	403187	403186	403186	403186	403186	403186	403190
	$\hat{\sigma}_{\alpha\alpha}$	2706.1	2612.6	2594.4	2587.9	2585.0	2583.4	2582.4	2581.7	2581.3	2581.0	-
	$\hat{\sigma}_{\alpha z}$	-3.5070	-3.2390	-3.1880	-3.1722	-3.1656	-3.1622	-3.1604	-3.1592	-3.1585	-3.1579	-3.1560
	$\hat{\sigma}_{zz}$	-3.9198	-4.0225	-4.0154	-4.0109	-4.0082	-4.0063	-4.0048	-4.0035	-4.0024	-4.0016	-3.997
	$\hat{\Phi}$	0.3263	0.3164	0.3143	0.3136	0.3132	0.3131	0.3129	0.3129	0.3128	0.3128	0.3127
	\hat{D}_z	-121.54	-16.278	-9.6342	-8.5184	-8.2038	-8.0807	-8.0178	-7.9754	-7.9386	-7.9020	-5.495
		Actuator Case										
	Mesh	2×8	4×16	6×24	8×32	10×40	12×48	14×56				<i>Analytical</i> [Cinefra et al., 2015a]
LW4	\hat{w}	5.5422	5.5420	5.5419	5.5418	5.5418	5.5418	5.5418				5.5418
	$\hat{\sigma}_{\alpha\alpha}$	-0.2048	-0.2119	-0.2132	-0.2137	-0.2140	-0.2141	-0.2141				-
	$\hat{\sigma}_{\alpha z}$	-0.6069	-0.5559	-0.5466	-0.5439	-0.5427	-0.5422	-0.5419				-0.5423
	$\hat{\sigma}_{zz}$	0.0390	-0.3508	-0.3370	-0.3438	-0.3742	-0.4104	-0.4417				-0.5571
	$\hat{\Phi}$	0.5009	0.5009	0.5009	0.5009	0.5009	0.5009	0.5009				0.5009
	\hat{D}_z	-36.201	-36.203	-36.207	-36.208	-36.209	-36.209	-36.209				-36.209

Different Variable Kinematic models have been used to perform the analysis of the shell structures. The acronyms have been modified adding a subscript to them, for the sake of clarity the list of subscripts is given below:

- $Case1 = \{layer1\} \{layer2, layer3\}$
- $Case2 = \{layer1, layer2\} \{layer3\}$

The results are listed in Table 8 for the sensor case, and in Table 9 for the actuator case. For the plate structures analyzed the following considerations can be drawn for the sensor cases and actuator cases. For both mechanical and electrical variables the variable kinematic configurations $EL4_{Case1}$, $EL4_{Case2}$ show an improvement of the solutions respect to the full equivalent single layer theory $EL4$. As demonstrated in the previous numerical example, it is preferable to model the piezoelectric skins of a multilayered structure with a layer-wise approach to obtain more accurate results. For this numerical example, the two possible variable kinematic theories $Case1$ and $Case2$ cannot be as accurate as the configuration with the piezoelectric skins modeled with a layer-wise approach, that for this three-layered structure is coincident with the full-layer wise model. The more accurate variable kinematic configuration is that which takes into account the layer-wise description of the layer subject to the mechanical or electrical load. For the sensor cases the $Case2$ configuration is more accurate, for the actuator cases the $Case1$ configuration is more close to the reference solution.

Table 8: Three-layer cylinder with a composite core and piezoelectric external skins. Mechanical and electrical variables described by Mono-models and Variable kinematic models for various radius to thickness ratios R/h . Sensor case.

	$R/h = 100$						$DOFs$
	\hat{w}	$\hat{\sigma}_{\alpha\alpha}$	$\hat{\sigma}_{\alpha z}$	$\hat{\sigma}_{zz}$	$\hat{\Phi}$	\hat{D}_z	
$LW4_a$ [Cinefra et al., 2015a]	403190	-	-3.1560	-3.997	0.3127	-5.495	
$LW4$	403185	2581.0	-3.1579	-4.0016	0.3128	-7.9020	343252
$LW1$	397196	2638.2	-2.9309	-3.8980	0.3081	-1600.8	105616
$EL3Z$	403237	2582.2	-3.1637	-3.9975	0.8662	-112.76	132020
$EL4$	403251	2580.8	-3.5091	-2.5532	0.8378	3648.5	132020
$EL3$	403251	2581.7	-3.5069	-2.5495	0.8664	3003.5	105616
$EL2$	405108	2546.2	-1.5952	-27.979	0.8724	-12631	79212
$EL1$	355114	3094.8	-1.6844	-25.846	0.0000	-25607	52808
$EL4_{Case1}$	403170	2580.9	-3.4019	-3.1394	0.4913	0.6731	237636
$EL4_{Case2}$	403214	2561.5	-3.1384	-2.7264	0.7887	513.47	237636
$EL3_{Case1}$	403164	2580.9	-3.7731	-2.1040	0.5107	3.0502	184828
$EL3_{Case2}$	403235	2580.9	-3.0706	-1.9132	0.9247	2531.1	184828
$EL2_{Case1}$	403131	2580.7	-2.2146	-6.0200	0.6671	0.3341	132020
$EL2_{Case2}$	403186	2592.1	-2.8999	-7.3777	1.0618	972.84	132020
$EL1_{Case1}$	388319	2575.6	-2.1355	102.05	0.2198	-213.08	79212
$EL1_{Case2}$	393626	2843.8	-2.0230	-147.95	0.1272	-38700	79212
	$R/h = 2$						$DOFs$
	\hat{w}	$\hat{\sigma}_{\alpha\alpha}$	$\hat{\sigma}_{\alpha z}$	$\hat{\sigma}_{zz}$	$\hat{\Phi}$	\hat{D}_z	
$LW4_a$ [Cinefra et al., 2015a]	30.225	-	-0.1193	-0.415	0.00497	0.752	
$LW4$	30.225	1.2065	-0.1194	-0.4150	0.00497	0.7348	343252
$LW1$	31.598	1.4335	-0.1143	-0.4047	0.00714	-2.5374	105616
$EL3Z$	30.162	1.4929	-0.1163	-0.3957	0.01110	-9.9503	132020
$EL4$	27.653	1.0410	-0.1275	-0.5243	-0.02601	16.025	132020
$EL3$	27.839	1.9639	-0.1246	-0.4625	0.01396	13.033	105616
$EL2$	16.090	0.3806	-0.0500	-0.1429	0.02323	-12.100	79212
$EL1$	16.373	0.5292	-0.0506	-0.1539	0.00000	-31.931	52808
$EL4_{Case1}$	28.508	1.1485	-0.1211	-0.4757	-0.0577	0.6670	237636
$EL4_{Case2}$	29.402	1.3944	-0.1208	-0.4218	0.0165	2.2707	237636
$EL3_{Case1}$	27.943	1.0920	-0.1256	-0.5498	-0.0586	0.6076	184828
$EL3_{Case2}$	29.292	1.4955	-0.1248	-0.4048	0.0246	3.9826	184828
$EL2_{Case1}$	24.031	0.8845	-0.0835	-0.1615	0.0035	0.5862	132020
$EL2_{Case2}$	27.241	1.4981	-0.0956	-0.4982	0.0320	8.6203	132020
$EL1_{Case1}$	18.060	1.0674	-0.0632	-0.1374	0.0050	-1.5134	79212
$EL1_{Case2}$	25.976	0.0759	-0.0801	-0.3057	0.0046	-55.425	79212

Table 9: Three-layer cylinder with a composite core and piezoelectric external skins. Mechanical and electrical variables described by Mono-models and Variable kinematic models for various radius to thickness ratios R/h . Actuator case.

	$R/h = 100$						$DOFs$
	\hat{w}	$\hat{\sigma}_{\alpha\alpha}$	$\hat{\sigma}_{\alpha z}$	$\hat{\sigma}_{zz}$	$\hat{\Phi}$	$\hat{\mathcal{D}}_z$	
$LW4_a$ [Cinefra et al., 2015a]	5.5418	-	-0.5423	-0.5571	0.5009	-36.209	
$LW4$	5.5418	-0.2141	-0.5419	-0.4417	0.5009	-36.209	170404
$LW1$	5.4331	-0.1833	-0.5080	-0.4459	0.5000	-34.865	52432
$EL3Z$	1.8837	-0.9776	-0.4124	830.44	0.5000	-141.81	65540
$EL4$	92.747	19.424	-202.29	-15334	0.5010	3724.6	65540
$EL3$	92.691	19.534	-203.24	-15337	0.5002	3745.2	52432
$EL2$	2520.2	-64.432	486.90	-141817	0.5066	-14300	39324
$EL1$	2250.4	-61.527	483.72	-141707	0.5000	-14451	26216
$EL4_{Case1}$	-3.1798	-0.2202	-2.6406	-1.6166	0.3224	-44.401	117972
$EL4_{Case2}$	26.953	0.9671	-124.78	15.979	0.6785	50.273	117972
$EL3_{Case1}$	-5.6162	-0.1922	-4.0188	-2987.5	0.2561	-51.697	91756
$EL3_{Case2}$	41.196	5.4375	-293.32	-2943.7	0.7453	1073.7	91756
$EL2_{Case1}$	-2.4141	-0.1676	-3.1852	-1083.3	0.2810	-52.076	65540
$EL2_{Case2}$	37.439	6.2793	337.58	-1117.0	0.7191	1400.4	65540
$EL1_{Case1}$	-1364.0	0.6154	-72.913	-113980	0.5516	-1636.7	39324
$EL1_{Case2}$	4140.8	-59.763	736.08	-125596	0.4490	-15022	39324
	$R/h = 2$						$DOFs$
	\hat{w}	$\hat{\sigma}_{\alpha\alpha}$	$\hat{\sigma}_{\alpha z}$	$\hat{\sigma}_{zz}$	$\hat{\Phi}$	$\hat{\mathcal{D}}_z$	
$LW4_a$ [Cinefra et al., 2015a]	-1.306	-	19.176	-116.36	0.4058	-106.61	
$LW4$	-1.306	-0.1759	19.208	-116.49	0.4058	-106.64	170404
$LW1$	-1.366	0.8046	11.078	-79.83	0.4916	-61.79	52432
$EL3Z$	-0.425	-0.5514	12.571	1044.0	0.4675	-211.86	65540
$EL4$	-3.137	0.5679	-156.43	-255.73	0.5486	-36.31	65540
$EL3$	-1.861	1.0151	-217.99	-622.17	0.4778	3.62	52432
$EL2$	-12.84	-0.9158	571.77	-3914.7	0.5395	-254.03	39324
$EL1$	-12.62	-1.9369	606.79	-3745.8	0.5000	-301.24	26216
$EL4_{Case1}$	-1.249	-0.1742	19.120	-116.75	0.2831	-106.72	117972
$EL4_{Case2}$	-3.281	0.1703	-73.019	-136.42	0.6549	-103.57	117972
$EL3_{Case1}$	-1.199	-0.1714	18.647	-155.50	0.2518	-106.74	91756
$EL3_{Case2}$	-3.728	0.5372	-279.71	174.84	0.7918	-69.74	91756
$EL2_{Case1}$	-0.949	-0.1750	-6.798	-106.46	0.2743	-107.49	65540
$EL2_{Case2}$	-7.025	0.6781	346.93	-1318.3	0.6902	-33.85	65540
$EL1_{Case1}$	-5.393	0.5046	104.25	-2031.9	0.5432	-80.87	39324
$EL1_{Case2}$	-11.69	-1.6581	643.28	-3892.4	0.4521	-319.48	39324

7.3 Four-layer cylindrical shell

A four-layer composite cylindrical shell with a Gr/Ep composite core [90°/0°] and PZT-4 piezoelectric external skins, see Figure 15, simply-supported boundary condition is considered. The static analysis of the shell structure is evaluated in sensor and actuator configuration. The material properties of the cylinder are given in Table 1. For all the cases the geometrical data are the same of the previous numerical subsection. In respect to the total thickness, a single piezoelectric skin is thick $h_p = 0.1h_{tot}$, while the single composite core layer is thick $h_c = 0.4h_{tot}$. The results are presented for different radius to thickness ratios $R_\beta/h = 2, 4, 10, 100$. The applied load is the same of the previous numerical example, due to the geometrical symmetry of the cylinder, the symmetry of the load pressure and boundary condition, an octave of the cylinder is analyzed, half cylinder along the α axis direction and a quarter along the β circumferential axis direction. For the sensor case a mesh grid of 20×80 , and for the actuator case a mesh grid of 14×56 elements are employed as the previous example of the three-layered cylinder.

The results are calculated in the following positions with the following form for the sensor cases:

$$\begin{aligned} \hat{w}(\alpha, \beta, z) &= w(a/2, 0, 0) * 10^9 & , & \quad \hat{\sigma}_{\alpha\alpha}(\alpha, \beta, z) = \sigma_{\alpha\alpha}(a/2, 0, +h/2) \\ \hat{\sigma}_{\alpha z}(\alpha, \beta, z) &= \sigma_{\alpha z}(a, 0, 0^-) & , & \quad \hat{\sigma}_{zz}(\alpha, \beta, z) = \sigma_{zz}(a/2, 0, -h/2) \\ \hat{\Phi}(\alpha, \beta, z) &= \Phi(a/2, 0, 0) & , & \quad \hat{\mathcal{D}}_z(\alpha, \beta, z) = \mathcal{D}_z(a/2, 0, +h/2) * 10^{11} \end{aligned}$$

For the actuator cases the variables are evaluated in the following form:

$$\begin{aligned} \hat{w}(\alpha, \beta, z) &= w(a/2, 0, 0) * 10^{11} & , & \quad \hat{\sigma}_{\alpha\alpha}(\alpha, \beta, z) = \sigma_{\alpha\alpha}(a/2, 0, +h/2) \\ \hat{\sigma}_{\alpha z}(\alpha, \beta, z) &= \sigma_{\alpha z}(a, 0, 0^-) & , & \quad \hat{\sigma}_{zz}(\alpha, \beta, z) = \sigma_{zz}(a/2, 0, +h/2) \\ \hat{\Phi}(\alpha, \beta, z) &= \Phi(a/2, 0, 0) & , & \quad \hat{\mathcal{D}}_z(\alpha, \beta, z) = \mathcal{D}_z(a/2, 0, +h/2) * 10^9 \end{aligned}$$

Different Variable Kinematic models have been used to perform the analysis of the shell structures. The acronyms have been modified adding a subscript to them, for the sake of clarity the list of subscripts is given below:

- $Case1 = \{layer1\} \{layer2, layer3, layer4\}$
- $Case2 = \{layer1, layer2, layer3\} \{layer4\}$
- $Case3 = \{layer1\} \{layer2, layer3\} \{layer4\}$

The results are listed in Table 10 for the sensor case, and in Table 11 for the actuator case. For the cylindrical shell structures analysed the following considerations can be drawn for the sensor cases:

- For big radius to thickness ratios $R/h = 100$ regarding the transverse displacement w , the theories $EL4_{Case1}$, $EL4_{Case2}$ and $EL4_{Case3}$ lead an improvement of the solution respect to the $EL4$ with different levels of accuracy, see Figure 16a. For small radius to thickness ratios $R/h = 2$, the in-plane stress $\sigma_{\alpha\alpha}$ is well described along the thickness, except from the $EL4_{Case1}$ and the full equivalent-single-layer theory $EL4$, those theories have a loss in accuracy for the description of the loaded lower layer, see Figure 16b.
- For both the transverse shear stress $\sigma_{\alpha z}$, see Figure 17a, and the transverse normal stress σ_{zz} , see Figure 17b, the theories $EL4_{Case1}$ and $EL4_{Case2}$ improve the results respect to the $EL4$ theory only in the layer with a layer-wise description. The $EL4_{Case3}$ theory is able to approximate very well along the entire thickness of the plate the full layer-wise reference solution $LW4$.
- Regarding the electric potential Φ , for big radius to thickness ratios $R/h = 100$, the theories $EL4_{Case1}$, $EL4_{Case2}$ and $EL4$ theories overestimate the reference solution, see Figure 18a. For the electric transverse displacement \mathcal{D}_z , for small radius to thickness ratios $R/h = 2$, see Figures 18b, the theories $EL4_{Case1}$ and $EL4_{Case2}$ improve the results respect to the $EL4$ theory only in the layer with a layer-wise description. The $EL4_{Case3}$ theory is the best approximating theory respect to the full layer-wise reference solution $LW4$.

For the cylindrical shell structures analysed in actuator configuration, the following considerations can be drawn:

- Regarding the transverse displacement w , for big radius to thickness ratios $R/h = 100$, the variable kinematic theories show different levels of accuracy, see Figure 19a, the $EL4,Case3$ solution is closer than $EL4,Case1$ and $EL4,Case2$ theories to the full layer-wise reference solution $LW4$. For small radius to thickness ratios $R/h = 2$ the in-plane stress $\sigma_{\alpha\alpha}$ is well described along the thickness only from the $EL4,Case3$ theory, the other theories have a loss in accuracy especially in loaded upper layer, see Figure 19b.
- For both the transverse shear stress $\sigma_{\alpha z}$, see Figure 20a, and the transverse normal stress σ_{zz} , see Figure 20b, the same considerations as the sensor cases can be depicted. The theories $EL4,Case1$ and $EL4,Case2$ improve the results respect to the $EL4$ theory only in the layer with a layer-wise description. The $EL4,Case3$ theory is able to approximate very well along the entire thickness of the plate the full layer-wise reference solution $LW4$.
- Regarding the electric potential Φ , for big radius to thickness ratios $R/h = 100$, see Figure 21a, the theories $EL4,Case1$, $EL4,Case2$ and $EL4$ theories can underestimate and overestimate the solution in the central composite layers. The $EL4,Case3$ theory is able to approximate very well the full layer-wise reference solution $LW4$.
- For the electric transverse displacement \mathcal{D}_z , for small radius to thickness ratios $R/h = 2$, see Figures 21b, the theories $EL4,Case1$ and $EL4,Case2$ improve the results respect to the $EL4$ theory only in the layer with a layer-wise description. The $EL4,Case3$ theory is the best approximating theory respect to the full layer-wise reference solution $LW4$.

The euclidean norm, as defined in equation 31, is a global indicator of the solution accuracy, it can be related to the reduction of degrees of freedom (dofs) of the structure model, in other words the euclidean norm can be related to the computational cost of the used models. In Figure 22 various mono-models and variable-kinematic models with different expansion order are related to the reduction dofs % respect to the adopted reference solution $LW4$ with the following definition:

$$reduction\ dofs\ \% = \frac{100 (DOFS_{LW4} - DOFS)}{DOFS_{LW4}} \quad (36)$$

It is taken into account the error norm of the transverse mechanical displacement \hat{w} for the actuator case of the shell with $R/h = 2$ ratio. It is evident, from figure 22, that as expected the solution accuracy grows with the increasing of the polynomial order with a convergence to the fourth-order. The ESL mono-models have the biggest dofs reduction coupled with large solution errors. Differently LW models have the biggest solution accuracy coupled with low dofs reductions. It is noticeable that variable-kinematic Case 1 models are able to have reduced solution errors because they are describing with layer-wise approach the loaded top layer. Differently variable-kinematic Case 2 models represent the worst solution for both accuracy and dofs reduction. Therefore, variable-kinematic Case 3 models describe very accurate results comparable with the LW models, with noticeable dofs reduction.

Table 10: Four-layer cylinder with a composite core and piezoelectric external skins. Mechanical and electrical variables described by Mono-models and Variable kinematic models for various radius to thickness ratios R/h . Sensor case.

	$R/h = 100$						$DOFs$
	\hat{w}	$\hat{\sigma}_{\alpha\alpha}$	$\hat{\sigma}_{\alpha z}$	$\hat{\sigma}_{zz}$	$\hat{\Phi}$	$\hat{\mathcal{D}}_z$	
$LW4_a$ [Carrera and Brischetto, 2007]	4403.2	-	-	-32549	0.3414	227910	
$LW4M_a$ [Carrera and Brischetto, 2007]	4403.2	-	-	-1.0000	0.3414	227910	
$LW4FM_a$ [Carrera and Brischetto, 2007]	4403.2	-	-	-0.9999	0.3414	-2.4676	
$LW4$	4403.1	2716.7	-0.6654	-0.9985	0.3416	-4.0092	448868
$LW1$	4387.1	2812.3	-2.5224	-260.44	0.3403	-1764.8	132020
$EL3Z$	4401.8	2710.2	-2.3028	-46.243	0.5404	-154.76	132020
$EL4$	4402.1	2741.2	-2.1376	-57.284	0.9333	2141.3	132020
$EL3$	4401.9	2715.0	-2.2215	-20.875	0.9488	1407.3	105616
$EL2$	4403.5	2684.2	-1.1480	55.766	0.9506	-5722.9	79212
$EL1$	3813.1	3256.8	-1.3543	-2176.7	0.0000	-20590	52808
$EL4_{Case 1}$	4402.2	2716.3	-1.6024	-89.931	0.6519	10.560	237636
$EL4_{Case 2}$	4402.4	2725.2	-1.5633	-0.9991	0.7804	522.82	237636
$EL4_{Case 3}$	4402.6	2716.4	-1.3976	-0.9987	0.3415	-4.0166	343252
$EL3_{Case 1}$	4401.4	2715.9	-2.2183	24.322	0.6849	15.898	184828
$EL3_{Case 2}$	4402.6	2734.7	-1.7344	-0.9988	0.8974	2304.4	184828
$EL3_{Case 3}$	4402.2	2716.3	-1.3883	-0.9986	0.3415	-4.0260	264040
$EL2_{Case 1}$	4400.6	2715.2	-1.7809	7.2858	0.8519	13.417	132020
$EL2_{Case 2}$	4402.3	2712.3	-1.9502	-1.2046	1.0438	315.94	132020
$EL2_{Case 3}$	4401.8	2715.9	-2.0836	-1.2042	0.3415	-3.5428	184828
$EL1_{Case 1}$	4226.9	2724.1	-1.6474	-1249.3	0.2146	478.46	79212
$EL1_{Case 2}$	4246.2	2975.9	-1.5025	-252.10	0.1699	-33077	79212
$EL1_{Case 3}$	4323.2	2773.2	-2.2237	-256.67	0.3354	-1739.1	105616
	$R/h = 2$						$DOFs$
	\hat{w}	$\hat{\sigma}_{\alpha\alpha}$	$\hat{\sigma}_{\alpha z}$	$\hat{\sigma}_{zz}$	$\hat{\Phi}$	$\hat{\mathcal{D}}_z$	
$LW4_a$ [Carrera and Brischetto, 2007]	0.2633	-	-	-2.2444	0.0039	9.8912	
$LW4M_a$ [Carrera and Brischetto, 2007]	0.2633	-	-	-1.0013	0.0039	9.8858	
$LW4FM_a$ [Carrera and Brischetto, 2007]	0.2633	-	-	-1.0013	0.0039	0.6092	
$LW4$	0.2633	1.0152	-0.0765	-1.0010	0.0038	0.5929	448868
$LW1$	0.2582	1.1101	-0.0706	-2.6056	0.0035	-2.4079	132020
$EL3Z$	0.2369	1.8632	-0.1103	-2.1548	0.1037	22.094	132020
$EL4$	0.2415	0.8268	-0.1152	-0.3013	-0.0269	14.010	132020
$EL3$	0.2371	1.6585	-0.1075	-2.1536	0.0107	8.5755	105616
$EL2$	0.1416	0.1893	-0.0385	-2.2960	0.0147	-5.8960	79212
$EL1$	0.1468	0.0882	-0.0391	-2.3340	0.0000	-22.409	52808
$EL4_{Case 1}$	0.2471	0.9560	-0.1028	0.2054	-0.0547	0.5236	237636
$EL4_{Case 2}$	0.2569	1.1699	-0.1071	-1.0010	0.0129	1.6966	237636
$EL4_{Case 3}$	0.2617	1.0081	-0.1010	-1.0010	0.0038	0.5880	343252
$EL3_{Case 1}$	0.2377	0.9327	-0.1044	-1.4773	-0.0512	0.5090	184828
$EL3_{Case 2}$	0.2577	1.2839	-0.1177	-1.0131	0.0196	2.9519	184828
$EL3_{Case 3}$	0.2622	1.0222	-0.1010	-1.0133	0.0039	0.6057	264040
$EL2_{Case 1}$	0.1860	0.5272	-0.0664	-2.4012	0.0079	0.2537	132020
$EL2_{Case 2}$	0.2448	1.2798	-0.0804	-1.0996	0.0234	7.6853	132020
$EL2_{Case 3}$	0.2631	0.9789	-0.0974	-1.1102	0.0035	0.6479	184828
$EL1_{Case 1}$	0.1631	0.8048	-0.0544	-2.1771	0.0031	-1.4746	79212
$EL1_{Case 2}$	0.2167	-0.4708	-0.0564	-2.1445	0.0050	-36.727	79212
$EL1_{Case 3}$	0.2702	1.0339	-0.0951	-2.5063	0.0054	-2.2854	105616

Table 11: Four-layer cylinder with a composite core and piezoelectric external skins. Mechanical and electrical variables described by Mono-models and Variable kinematic models for various radius to thickness ratios R/h . Actuator case.

	$R/h = 100$						$DOFs$
	\hat{w}	$\hat{\sigma}_{\alpha\alpha}$	$\hat{\sigma}_{\alpha z}$	$\hat{\sigma}_{zz}$	$\hat{\Phi}$	\hat{D}_z	
$LW4_a$ [Carrera and Brischetto, 2007]	2.4869	-	-	-0.1835	0.5009	-0.3494	
$LW4M_a$ [Carrera and Brischetto, 2007]	2.4869	-	-	0.0000	0.5009	-0.3494	
$LW4FM_a$ [Carrera and Brischetto, 2007]	2.4869	-	-	0.0000	0.5009	-0.3622	
$LW4$	2.4872	-0.2902	0.0000	0.0000	0.5009	-0.3621	222836
$LW1$	2.4452	-0.2596	-0.0001	0.0318	0.5009	-0.3485	65540
$EL3Z$	43.5403	18.077	-0.0018	-48.670	0.4959	37.190	65540
$EL4$	44.3032	18.006	-0.0163	-48.710	0.5009	37.136	65540
$EL3$	44.8222	18.157	-0.0098	-48.878	0.5001	37.343	52432
$EL2$	1124.5	-91.270	0.0690	53.830	0.5034	-133.35	39324
$EL1$	1029.2	-90.429	0.0657	59.038	0.5000	-134.39	26216
$EL4_{Case 1}$	-12.287	-0.4031	-0.0003	0.0000	0.3224	-0.4440	117972
$EL4_{Case 2}$	22.269	0.7975	-0.0120	-0.1312	0.6784	0.5026	117972
$EL4_{Case 3}$	2.4880	-0.2902	0.0000	0.0000	0.5009	-0.3621	170404
$EL3_{Case 1}$	-17.722	-0.4577	-0.0004	0.0000	0.2562	-0.5169	91756
$EL3_{Case 2}$	34.832	5.1907	-0.0214	-14.279	0.7452	10.731	91756
$EL3_{Case 3}$	2.4889	-0.2902	0.0000	0.0000	0.5009	-0.3621	131080
$EL2_{Case 1}$	-14.717	-0.4399	-0.0003	0.0000	0.2811	-0.5207	65540
$EL2_{Case 2}$	29.364	6.0191	0.0441	-19.827	0.7190	13.997	65540
$EL2_{Case 3}$	2.4880	-0.2903	0.0000	0.0000	0.5009	-0.3621	91756
$EL1_{Case 1}$	-2200.3	-18.715	-0.0044	-1.2398	0.5494	-15.798	39324
$EL1_{Case 2}$	3493.6	-75.394	0.1000	97.022	0.4510	-143.38	39324
$EL1_{Case 3}$	2.4558	-0.2596	0.0000	0.0318	0.5000	-0.3485	52432
	$R/h = 2$						$DOFs$
	\hat{w}	$\hat{\sigma}_{\alpha\alpha}$	$\hat{\sigma}_{\alpha z}$	$\hat{\sigma}_{zz}$	$\hat{\Phi}$	\hat{D}_z	
$LW4_a$ [Carrera and Brischetto, 2007]	-1.1542	-	-	0.1416	0.4064	-1.0754	
$LW4M_a$ [Carrera and Brischetto, 2007]	-1.1542	-	-	0.0000	0.4064	-1.0754	
$LW4FM_a$ [Carrera and Brischetto, 2007]	-1.1542	-	-	0.0000	0.4064	-1.0654	
$LW4$	-1.1534	-0.0894	-0.0022	0.0000	0.3962	-1.0659	222836
$LW1$	-1.2820	0.8799	0.0008	0.9183	0.3900	-0.6169	65540
$EL3Z$	-1.0226	0.3370	0.0031	1.1361	-1.1287	-0.9830	65540
$EL4$	-3.0789	0.7162	-0.0242	-0.2791	0.5529	-0.3374	65540
$EL3$	-0.8279	1.2289	-0.0318	-0.5882	0.4804	0.1053	52432
$EL2$	-12.269	-1.2000	0.0698	1.1274	0.5332	-2.4689	39324
$EL1$	-12.680	-2.6283	0.0818	0.0327	0.5000	-2.7931	26216
$EL4_{Case 1}$	-1.0742	-0.0860	-0.0029	0.0000	0.2769	-1.0667	117972
$EL4_{Case 2}$	-2.9077	0.3489	-0.0195	0.5244	0.6574	-1.0222	117972
$EL4_{Case 3}$	-1.1401	-0.0887	-0.0027	0.0000	0.3962	-1.0659	170404
$EL3_{Case 1}$	-1.1021	-0.0847	-0.0028	0.0022	0.2478	-1.0668	91756
$EL3_{Case 2}$	-3.6975	0.7041	-0.0351	0.3716	0.8013	-0.6621	91756
$EL3_{Case 3}$	-1.1377	-0.0849	-0.0028	0.0022	0.3967	-1.0654	131080
$EL2_{Case 1}$	-0.6215	-0.0647	-0.0062	-0.0171	0.2741	-1.0740	65540
$EL2_{Case 2}$	-7.1876	0.5386	0.0363	-0.4764	0.6981	-0.2952	65540
$EL2_{Case 3}$	-1.1572	-0.0937	-0.0041	-0.0173	0.3943	-1.0729	91756
$EL1_{Case 1}$	-4.6472	0.4951	0.0103	0.8077	0.5429	-0.8084	39324
$EL1_{Case 2}$	-12.137	-2.2188	0.0890	0.9437	0.4528	-2.9806	39324
$EL1_{Case 3}$	-1.0557	0.9225	-0.0045	0.9191	0.4924	-0.6172	52432

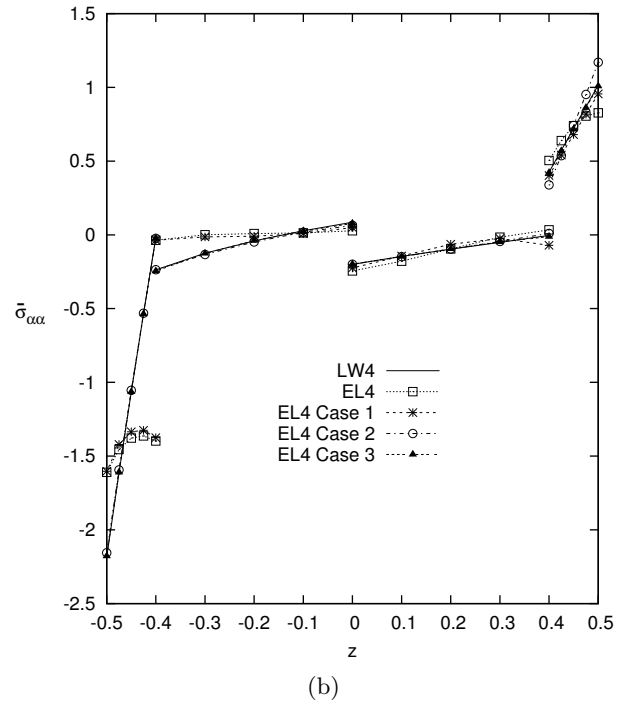
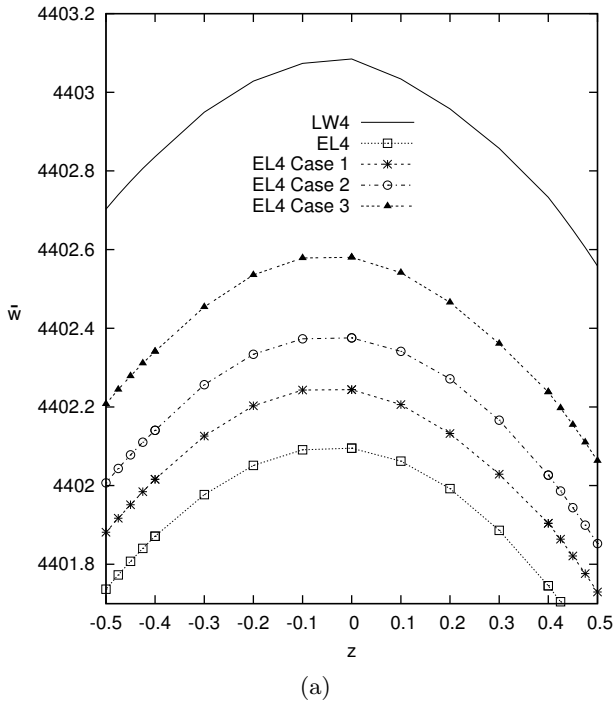


Figure 16: Four-layered cylinder, Sensor case, transverse mechanical displacement and in-plane stress, \hat{w} for $R/h = 100$ (a), $\hat{\sigma}_{\alpha\alpha}$ for $R/h = 2$ (b).

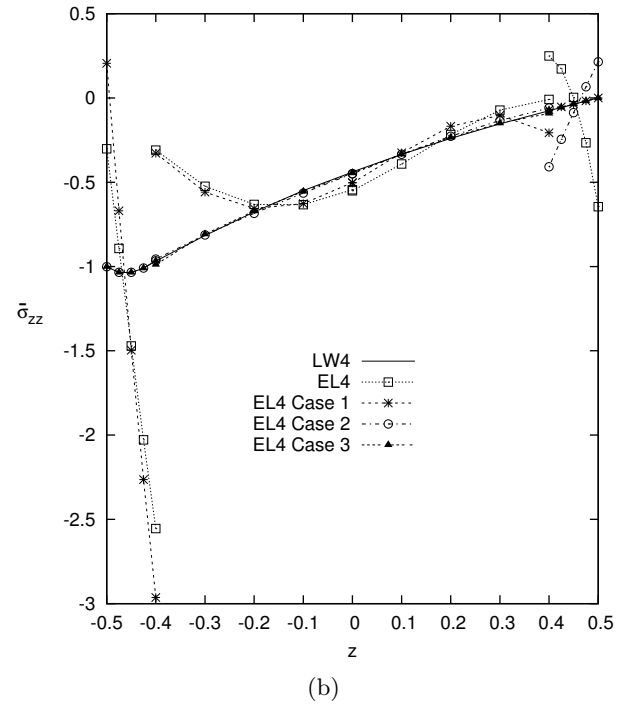
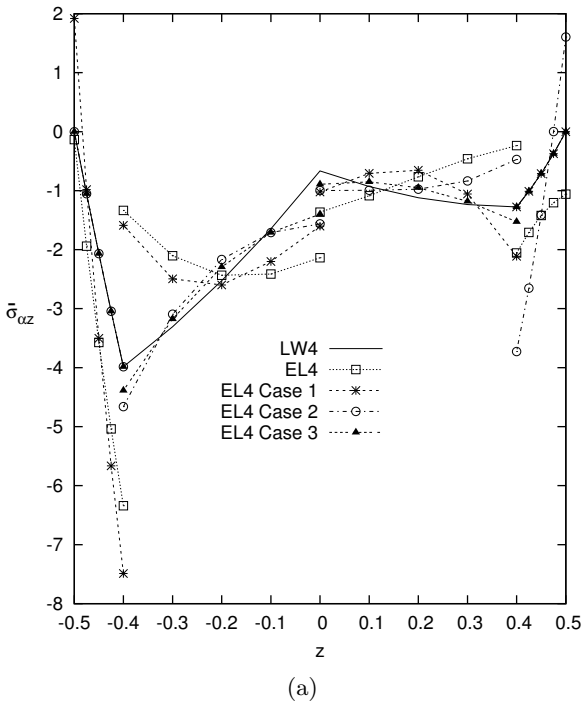


Figure 17: Four-layered cylinder, Sensor case, transverse mechanical stresses, $\hat{\sigma}_{\alpha z}$ for $R/h = 100$ ratio (a), $\hat{\sigma}_{zz}$ for $R/h = 2$ ratio (b).

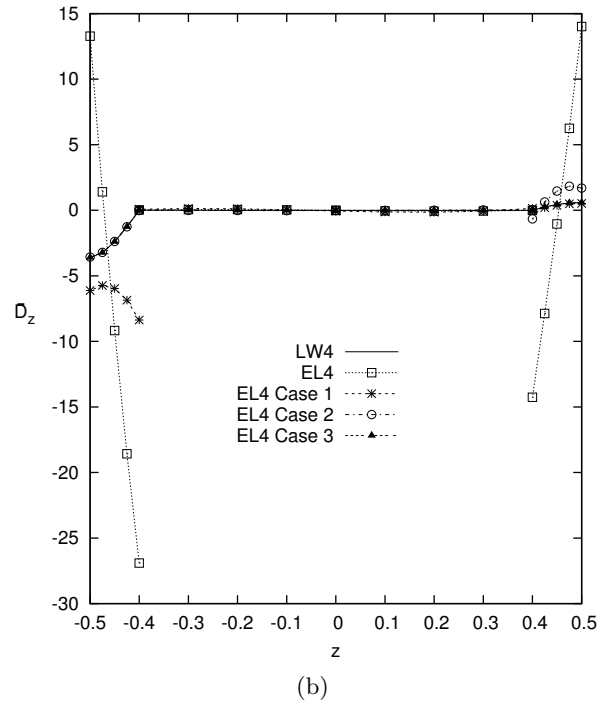
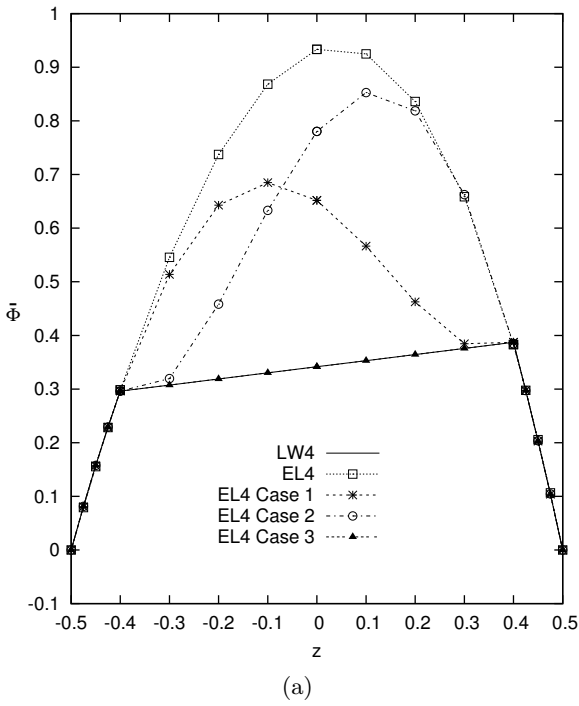


Figure 18: Four-layered cylinder, Sensor case, electric potential and transverse electric displacement, $\hat{\Phi}$ for $R/h = 100$ (a), and \hat{D}_z for $R/h = 2$ (b).

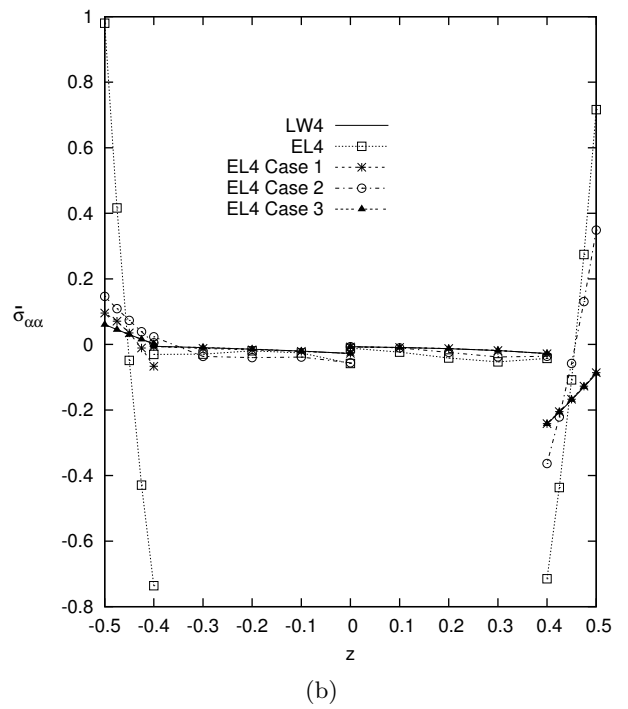
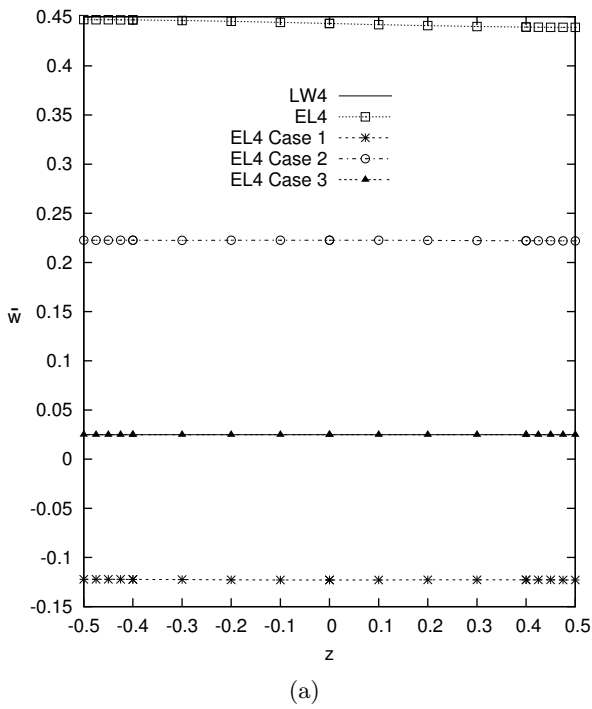


Figure 19: Four-layered cylinder, Actuator case, transverse mechanical displacement and in-plane stress, \hat{w} for $R/h = 100$ (a), $\hat{\sigma}_{\alpha\alpha}$ for $R/h = 2$ (b).

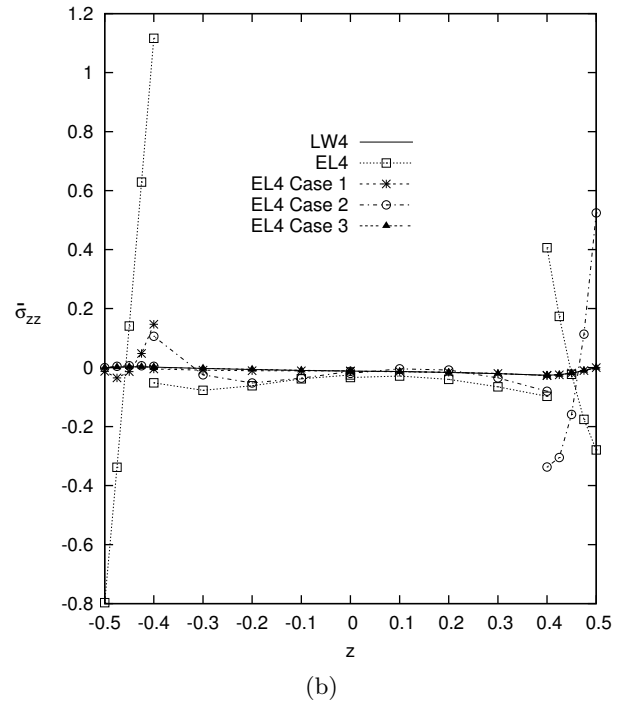
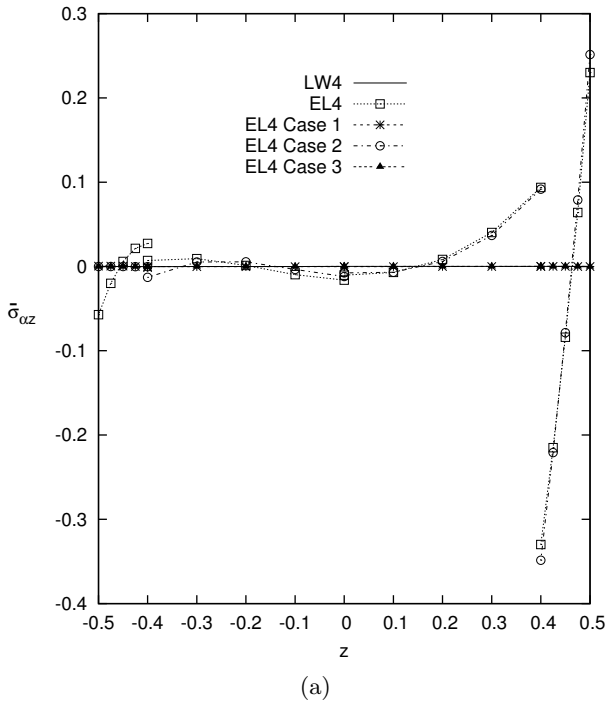


Figure 20: Four-layered cylinder, Actuator case, transverse mechanical stresses, $\hat{\sigma}_{\alpha z}$ for $R/h = 100$ ratio (a), $\hat{\sigma}_{zz}$ for $R/h = 2$ ratio (b).

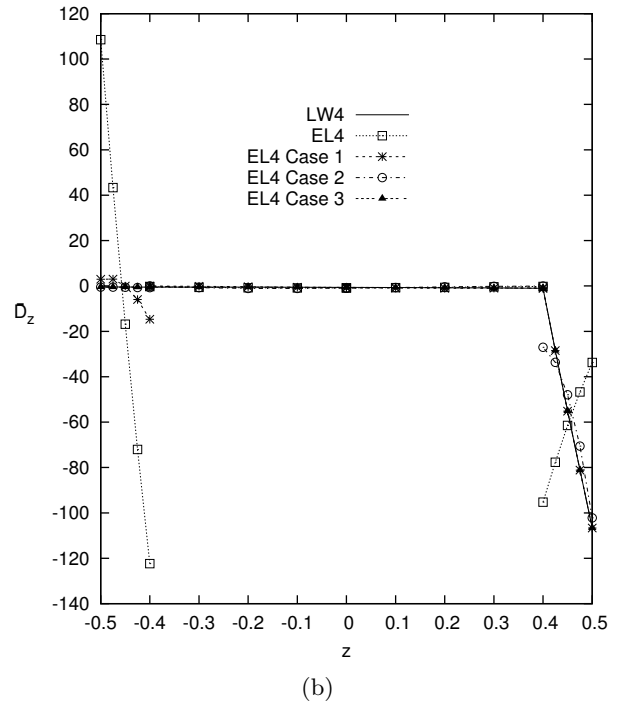
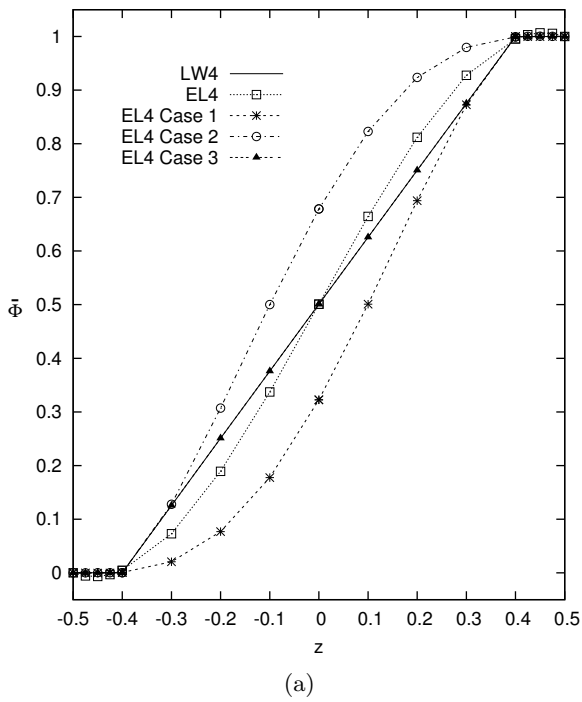


Figure 21: Four-layered cylinder, Actuator case, electric potential and transverse electric displacement, $\hat{\Phi}$ for $R/h = 100$ (a), and \hat{D}_z for $R/h = 2$ (b).

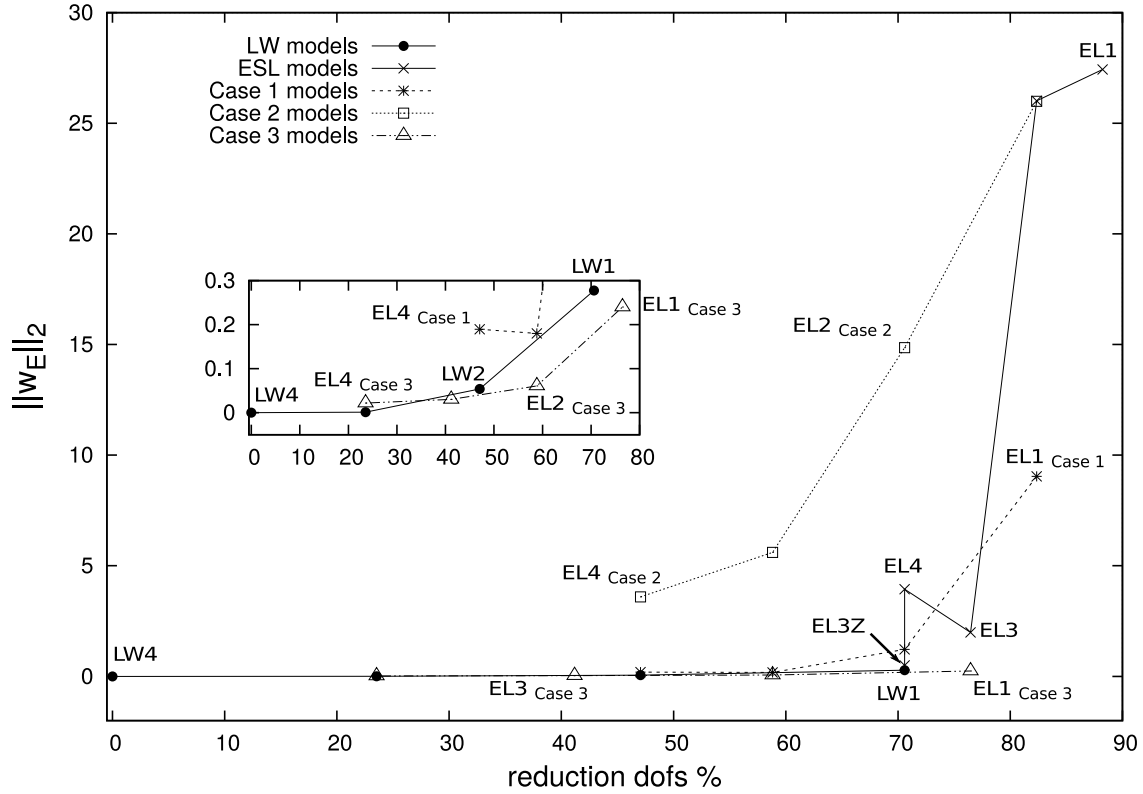


Figure 22: Four-layered cylinder, Actuator case, Euclidean Norm Error of the transverse mechanical displacement, \hat{w} for $R/h = 2$.

8 Conclusions

This paper has dealt with the static analysis of composite plates and shells embedded with piezoelectric layers using a two-dimensional finite element based on the Unified Formulation. The element has been assessed by analyzing cross-ply plates with piezoelectric skins under bi-sinusoidal mechanical or electrical loads and simply-supported boundary conditions, multilayered composite shells with piezoelectric skins under bi-sinusoidal mechanical or electrical loads and simply-supported boundary conditions. The results have been presented in terms of both transverse displacement, in-plane stresses, transverse shear stresses, transverse normal stress, electric potential and transverse electric displacement for various thickness ratios and radius to thickness ratios. The performances of the shell element have been tested, and the different theories (classical, refined, and Variable-Kinematic models) within the CUF framework have been compared. The following conclusions can be drawn:

1. The shell element with the MITC technique is locking free, for all the considered cases and all the chosen models. The results converge to the reference solution by increasing the order of expansion of the displacements in the thickness direction, independently from the employed function type.
2. For multilayered composite plate and multilayered shells, Variable-Kinematic models permit to improve the results with a reduction of computational costs, with respect to a full Layer-Wise solutions.
3. The piezoelectric skins have to be modeled by a layer-wise description. The Variable-Kinematic model permits to improve globally the results, and at the same time permits to reduce the computational cost of the analysis, assembling the composite core with an equivalent-single-layer model.

4. For multilayered structures, the shear stresses can be modeled, in specific layers, by Variable-Kinematic models with the same accuracy of Layer-Wise theories, whereas strong reduction of computational costs can be obtained in the other layers.

References

- [Auricchio et al., 2001] Auricchio, F., Bisegna, P., and Lovadina, C. (2001). Finite element approximation of piezoelectric plates. *International Journal for Numerical Methods in Engineering*, 50:1469–1499.
- [Ballhause et al., 2005] Ballhause, D., D’Ottavio, M., Kroplin, B., and Carrera, E. (2005). A unified formulation to assess multilayered theories for piezoelectric plates. *Computers & Structures*, 83(15-16):1217–1235.
- [Bathe and Brezzi, 1987] Bathe, K. J. and Brezzi, F. (1987). A simplified analysis of two plate bending elements-the MITC4 and MITC9 elements. *Proceedings, Numerical Methods in Engineering: Theory and Applications*.
- [Bathe and Dvorkin, 1986] Bathe, K. J. and Dvorkin, E. (1986). A formulation of general shell elements - the use of mixed interpolation of tensorial components. *International Journal for Numerical Methods in Engineering*, 22:697–722.
- [Bathe et al., 2003] Bathe, K. J., Lee, P. S., and Hiller, J. F. (2003). Towards improving the MITC9 shell element. *Computers and Structures*, 81:477–489.
- [Benjeddou et al., 2002] Benjeddou, A., Deu, J., and Letombe, S. (2002). Free vibrations of simply-supported piezoelectric adaptive plates: An exact sandwich formulation. *Thin-walled structures*, 40:573–666.
- [Botshekanan Dehkordi et al., 2013] Botshekanan Dehkordi, M., Cinefra, M., Khalili, S. M. R., and Carrera, E. (2013). Mixed LW/ESL models for the analysis of sandwich plates with composite faces. *Composite Structures*, 98:330–339.
- [Botshekanan Dehkordi et al., 2016] Botshekanan Dehkordi, M., Khalili, S. M. R., and Carrera, E. (2016). Non-linear transient dynamic analysis of sandwich plate with composite face-sheets embedded with shape memory alloy wires and flexible core- Based on the mixed LW (Layer-wise)/ESL (Equivalent single layer) models. *Composites Part B*, 87:59–74.
- [Carrera, 1999a] Carrera, E. (1999a). Multilayered shell theories accounting for layerwise mixed description, Part 1: governing equations. *AIAA Journal*, 37(9):1107–1116.
- [Carrera, 1999b] Carrera, E. (1999b). Multilayered shell theories accounting for layerwise mixed description, Part 2: numerical evaluations. *AIAA Journal*, 37(9):1117–1124.
- [Carrera, 2001] Carrera, E. (2001). Developments, ideas and evaluation based upon Reissner’s Mixed Variational Theorem in the Modeling of Multilayered Plates and Shells. *Applied Mechanics Review*, 54:301–329.
- [Carrera, 2002] Carrera, E. (2002). Theories and finite elements for multilayered, anisotropic, composite plates and shells. *Archives of Computational Methods in Engineering*, 9(2):87–140.
- [Carrera, 2003] Carrera, E. (2003). Theories and finite elements for multilayered plates and shells: a unified compact formulation with numerical assessment and benchmarking. *Archives of Computational Methods in Engineering*, 10(3):215–296.
- [Carrera and Boscolo, 2007] Carrera, E. and Boscolo, M. (2007). Classical and mixed finite elements for static and dynamic analysis of piezoelectric plates. *International Journal for Numerical Methods in Engineering*, 70:1135–1181.

- [Carrera et al., 2007] Carrera, E., Boscolo, M., and Robaldo, M. (2007). Hierarchic Multilayered Plate Elements for Coupled Multifield Problems of Piezoelectric Adaptive Structures: Formulation and Numerical Assessment. *Archives of Computational Methods in Engineering*, 14:383–430.
- [Carrera and Brischetto, 2007] Carrera, E. and Brischetto, S. (2007). Piezoelectric Shell Theories with a priori Continuous Transverse Electromechanical Variables. *Mechanics of Materials and Structures*, 2(2):377–398.
- [Carrera et al., 2010] Carrera, E., Brischetto, S., and Cinefra, M. (2010). Variable Kinematics and Advanced Variational Statements for Free Vibrations Analysis of Piezoelectric Plates and Shells. *Computer Modeling in Engineering & Sciences*, 65(3):259–341.
- [Carrera and Nali, 2010a] Carrera, E. and Nali, P. (2010a). Classical and Mixed Finite Plate Elements for the Analysis of Multifield Problems and Smart Layered Structures. *Acta Mechanica Sinica*, 23:115–121.
- [Carrera and Nali, 2010b] Carrera, E. and Nali, P. (2010b). Multilayered plate elements for the analysis of multifield problems. *Finite Element in Analysis and Design*, 46:732–742.
- [Carrera et al., 2017] Carrera, E., Pagani, A., and Valvano, S. (2017). Shell elements with through-the-thickness variable kinematics for the analysis of laminated composite and sandwich structures. *Composites Part B*, 111:294–314.
- [Carrera and Robaldo, 2010] Carrera, E. and Robaldo, M. (2010). Hierarchic finite elements based on a unified formulation for the static analysis of shear actuated multilayered piezoelectric plates. *Multidiscipline Modeling in Materials and Structures*, 6(1):45–77.
- [Chopra, 2000] Chopra, I. (2000). Status of application of smart structures technology to rotorcraft systems. *Journal of the American Helicopter Society*, 45:228–252.
- [Ciarlet and Gratie, 2005] Ciarlet, P. G. and Gratie, L. (2005). Another approach to linear shell theory and a new proof of Korn’s inequality on a surface. *Comptes rendus de l’Academie des Sciences Paris*, I,340:471–478.
- [Cinefra et al., 2015a] Cinefra, M., Carrera, E., and Valvano, S. (2015a). Variable Kinematic Shell Elements for the Analysis of Electro-Mechanical Problems. *Mechanics of Advanced Materials and Structures*, 22(1-2):77–106.
- [Cinefra et al., 2015b] Cinefra, M., Valvano, S., and Carrera, E. (2015b). A layer-wise MITC9 finite element for the free-vibration analysis of plates with piezo-patches. *International Journal of Smart and Nano Materials*, 6(2):85–104.
- [Cinefra et al., 2015c] Cinefra, M., Valvano, S., and Carrera, E. (2015c). Heat conduction and Thermal Stress Analysis of laminated composites by a variable kinematic MITC9 shell element. *Curved and Layered Structures*, 1:301–320.
- [Cinefra et al., 2016] Cinefra, M., Valvano, S., and Carrera, E. (2016). Thermal stress analysis of laminated structures by a variable kinematic MITC9 shell element. *Journal of Thermal Stresses*, 39(2):121–141.
- [D’Ottavio et al., 2006] D’Ottavio, M., Ballhause, D., Kroplin, B., and Carrera, E. (2006). Closed-form solutions for the free-vibration problem of multilayered piezoelectric shells. *Computers & Structures*, 84:1506–1524.

- [EerNisse, 1967] EerNisse, E. P. (1967). Variational method for electroelastic vibration analysis. *IEEE Transaction on Sonics and Ultrasonics*, 14(4):153–213.
- [Foster, 2009] Foster, D. (2009). The bridge to smart technology. In *Bloomberg Businessweek*.
- [Gaudenzi, 2009] Gaudenzi, P. (2009). Smart Structures: Physical Behaviour, Mathematical Modelling and Applications. *John Wiley & Sons, Ltd, UK*.
- [Heyliger et al., 1996] Heyliger, P., Pei, K. C., and Saravanos, D. A. (1996). Layerwise mechanics and finite element model for laminated piezoelectric shells. *AIAA Journal*, 34(11):2353–2413.
- [Huang, 1987] Huang, N. C. (1987). Membrane locking and assumed strain shell elements. *Computers and Structures*, 27(5):671–677.
- [Hughes et al., 1978] Hughes, T. J. R., Cohen, M., and Horaun, M. (1978). Reduced and selective integration techniques in the finite element methods. *Nuclear Engineering and Design*, 46:203–222.
- [Hughes and Tezduyar, 1981] Hughes, T. J. R. and Tezduyar, T. (1981). Finite elements based upon Mindlin plate theory with particular reference to the four-node isoparametric element. *Journal of Applied Mechanics*, 48:587–596.
- [Inman et al., 2001] Inman, D., Ahmadihan, M., and Claus, R. (2001). Simultaneous active damping and health monitoring of aircraft panels. *Journal of Intelligent Material Systems and Structures*, 12:775–783.
- [Jones et al., 1984] Jones, R., Callinan, R., Teh, K. K., and Brown, K. C. (1984). Analysis of Multi-Layer Laminates Using Three-Dimensional Super Elements. *International Journal for Numerical Methods in Engineering*, 20(3):583–587.
- [Kapuria, 2004] Kapuria, S. (2004). A coupled zig-zag third-order theory for piezoelectric hybrid cross-ply plates. *Journal of Applied Mechanics*, 71:604–618.
- [Klinkel and Wagner, 2008] Klinkel, S. and Wagner, W. (2008). A piezoelectric solid shell element based on a mixed variational formulation for geometrically linear and nonlinear applications. *Computers & Structures*, 86:38–46.
- [Koiter, 1970] Koiter, W. T. (1970). On the foundations of the linear theory of thin elastic shell. *Proceedings of the Koninklijke Nederlandse Akademie van Wetenschappen*, 73:169–195.
- [Kulikov and Plotnikova, 2011] Kulikov, G. M. and Plotnikova, S. V. (2011). Exact geometry piezoelectric solid-shell element based on the 7-parameter model. *Mechanics of Advanced Materials and Structures*, 18:133–146.
- [Marinković et al., 2009] Marinković, D., Köppe, H., and Gabbert, U. (2009). Aspects of Modeling Piezoelectric Active Thin-walled Structures. *Journal of Intelligent Material Systems and Structures*, 20(15):1835–1844.
- [Milazzo, A, 2014] Milazzo, A (2014). Refined equivalent single layer formulations and finite elements for smart laminates free vibrations. *Composites Part B*, 61:238–253.
- [Mindlin, 1952] Mindlin, R. D. (1952). Forced thickness-shear and flexural vibrations of piezoelectric crystal plates. *Journal of Applied Physics*, 23:83–91.
- [Murakami, 1986] Murakami, H. (1986). Laminated composite plate theory with improved in-plane responses. *Journal of Applied Mechanics*, 53:661–666.

- [Noor, 1972] Noor, A. K. (1972). Finite element analysis of anisotropic plates. *American Institute of Aeronautics and Astronautics Journal*, 11:289–307.
- [Noor and Burton, 1990] Noor, A. K. and Burton, W. S. (1990). Assessment of computational models for multi-layered composite shells. *Applied Mechanics Review*, 43:67–97.
- [Ossadzow-David and Touratier, 2004] Ossadzow-David, C. and Touratier, M. (2004). A multilayered piezoelectric shell theory. *Composites Science and Technology*, 64:2121–2158.
- [Pagani et al.,] Pagani, A., Valvano, S., and Carrera, E. Analysis of laminated composites and sandwich structures by variable-kinematic MITC9 plate elements. *Journal of Sandwich Structures and Materials*.
- [Pagano and Soni, 1983] Pagano, N. J. and Soni, S. R. (1983). Global-Local Laminate Variational Model. *International Journal of Solids and Structures*, 19(3):207–228.
- [Preumont et al., 2009] Preumont, A., Bastaitis, R., and Rodrigues, G. (2009). Active optics for large segmented mirrors: scale effects. *In Proceedings of the IV ECCOMAS Thematic Conference on Smart Structures and Materials*.
- [Pryor and Barker, 1971] Pryor, C. W. and Barker, R. M. (1971). A finite element analysis including transverse shear effect for applications to laminated plates. *American Institute of Aeronautics and Astronautics Journal*, 9:912–917.
- [Reddy, 1993] Reddy, J. N. (1993). An evaluation of equivalent-single-layer and layerwise theories of composite laminates. *Composite Structures*, 25:21–35.
- [Reddy, 1997] Reddy, J. N. (1997). Mechanics of laminated composite plates and shells. *Theory and Analysis*, CRC Press.
- [Reddy and Robbins, 1994] Reddy, J. N. and Robbins, D. H. (1994). Theories and computational models for composite laminates. *Applied Mechanics Review*, 47:147–165.
- [Robaldo et al., 2006] Robaldo, M., Carrera, E., and Benjeddou, A. (2006). A unified formulation for finite element analysis of piezoelectric adaptive plates. *Computers and Structures*, 84:1494–1505.
- [Rogacheva, 1994] Rogacheva, N. N. (1994). The theory of piezoelectric shells and plates. *Boca Raton: CRC Press*.
- [Roger, 2009] Roger, C. (2009). Intelligent material systems and structures. *In Proceedings of US Japan Workshop on Smart/Intelligent Materials and Systems*.
- [Saravanos and Heyliger, 1999] Saravanos, D. A. and Heyliger, P. R. (1999). Mechanics and computational models for laminated piezoelectric beams, plates and shells. *Applied Mechanics Review*, 52(10):305–324.
- [Sheikh et al., 2001] Sheikh, A. H., Topdar, P., and Halder, S. (2001). An appropriate FE model for through-thickness variation of displacement and potential in thin moderately thick smart laminates. *Computers & Structures*, 51:401–409.
- [Tiersten, 1969] Tiersten, H. F. (1969). Linear piezoelectric plate vibrations. *New York Plenum Press*.
- [Tiersten and Mindlin, 1962] Tiersten, H. F. and Mindlin, R. D. (1962). Forced vibrations of piezoelectric crystal plates. *Quarterly of Applied Mathematics*, 20(2):107–126.

- [Varadan and Bhaskar, 1997] Varadan, T. K. and Bhaskar, K. (1997). Review of different theories for the analysis of composites. *Journal of Aerospace Society of India*, 49:202–208.
- [Wang and Crossman, 1978] Wang, A. S. D. and Crossman, F. W. (1978). Calculation of Edge Stresses in Multi-Layer by Sub-Structuring. *Journal of Composite Materials*, 12:76–83.
- [Yasin and Kapuria, 2014] Yasin, Y. and Kapuria, S. (2014). An efficient finite element with layerwise mechanics for smart piezoelectric composite and sandwich shallow shells. *Computational Mechanics*, 53:101–124.